Cell

Argonautes Promote Male Fertility and Provide a Paternal Memory of Germline Gene Expression in *C. elegans*

Colin C. Conine,[1] James J. Moresco,[2] Weifeng Gu,[1] Masaki Shirayama,[1,3] Darryl Conte, Jr.,[1] John R. Yates III,[2] and Craig C. Mello[1,3,*]

[1]RNA Therapeutics Institute and Program in Molecular Medicine, University of Massachusetts Medical School, Worcester, MA 01605, USA
[2]Department of Chemical Physiology, 10550 North Torrey Pines Road, SR11, The Scripps Research Institute, La Jolla, CA 92037, USA
[3]Howard Hughes Medical Institute, Worcester, MA 01605, USA
*Correspondence: craig.mello@umassmed.edu
http://dx.doi.org/10.1016/j.cell.2013.11.032

SUMMARY

During each life cycle, germ cells preserve and pass on both genetic and epigenetic information. In *C. elegans*, the ALG-3/4 Argonaute proteins are expressed during male gametogenesis and promote male fertility. Here, we show that the CSR-1 Argonaute functions with ALG-3/4 to positively regulate target genes required for spermiogenesis. Our findings suggest that ALG-3/4 functions during spermatogenesis to amplify a small RNA signal that represents an epigenetic memory of male-specific gene expression. CSR-1, which is abundant in mature sperm, appears to transmit this memory to offspring. Surprisingly, in addition to small RNAs targeting male-specific genes, we show that males also harbor an extensive repertoire of CSR-1 small RNAs targeting oogenesis-specific mRNAs. Together, these findings suggest that *C. elegans* sperm transmit not only the genome but also epigenetic binary signals in the form of Argonaute/small RNA complexes that constitute a memory of gene expression in preceding generations.

INTRODUCTION

The transmission of information independently of the DNA sequence of the genome is termed epigenetic inheritance. During sexual reproduction, both genetic and epigenetic information is passed to the zygote via specialized germ cells known as gametes. Gametogenesis involves dynamic molecular and morphological changes, culminating in the creation of highly specialized sperm and egg cells that package a haploid genome and all of the cellular machinery and epigenetic information necessary to launch zygotic development upon fertilization. Although many of the pathways required for gametogenesis are phylogenetically conserved (Eddy, 2002), especially those that mediate the partitioning of genetic information, very little is known about how gametes package and transmit epigenetic inheritance.

Male gametogenesis is an amazing example of cellular differentiation in which undifferentiated male germ cells proceed through meiosis and develop into motile spermatozoa. In mammals, the process of spermiogenesis (when spermatids differentiate into highly polarized motile spermatozoa) is initiated by a massive wave of gene expression essential for postmeiotic differentiation (Sassone-Corsi, 2002). Shortly thereafter, transcription ceases, and compaction of the haploid male genome ensues. Genome compaction within differentiating spermatids is facilitated by the replacement in chromatin of histones with small basic proteins called protamines (Wykes and Krawetz, 2003).

The culmination of male gametogenesis is a motile gamete capable of initiating fertilization and delivering a paternal genome complement to an egg. However, genetic material is not the only information packaged in the sperm. Epigenetic information is also transmitted in the form of chromatin (DNA and/or histone) modifications and RNA. In humans and mice, paternal epigenetic factors have been shown to influence metabolism, stress response, and reproduction (Rando, 2012).

In *C. elegans*, epigenetic inheritance involves Argonaute/small RNA pathways. Argonautes are structurally related to ribonuclease H and gain sequence specificity via small guide RNAs. Upon binding, Argonautes can direct endonucleolytic cleavage of target mRNAs or can recruit cofactors that mediate posttranscriptional or transcriptional silencing (Ghildiyal and Zamore, 2009). In *C. elegans*, mutations that perturb Argonaute pathways often result in infertility (Batista et al., 2008; Buckley et al., 2012; Claycomb et al., 2009; Conine et al., 2010; Gu et al., 2009; Han et al., 2009; Pavelec et al., 2009). For example, the Piwi Argonaute PRG-1 is required for both male and hermaphrodite fertility and has been linked to transposon and transgene silencing (Batista et al., 2008; Ruby et al., 2006). PRG-1 engages over 30,000 distinct species of genomically encoded small RNAs, termed Piwi-interacting RNAs (piRNAs) (Batista et al., 2008; Gu et al., 2012). PRG-1/piRNA complexes are thought to utilize imperfect base-pairing to scan germline-expressed mRNAs (Bagijn et al., 2012; Lee et al., 2012). When PRG-1/piRNA complexes bind to foreign RNA sequences, such as those produced by a transgene, they initiate the production, via RNA-dependent RNA polymerase (RdRP), of amplified small

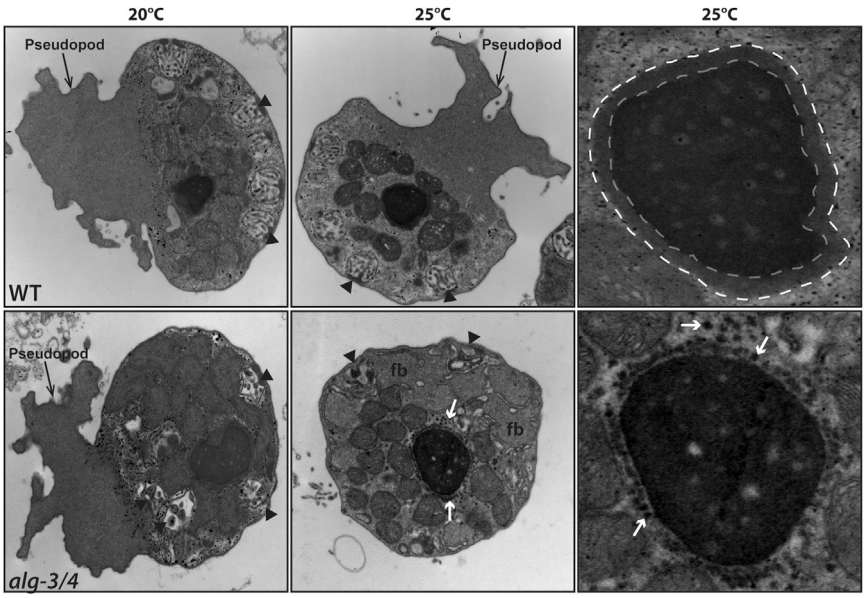

Figure 1. Ultrastructural Analysis of *alg-3/4* Spermatozoa

Transmission electron micrographs of spermatozoa from WT (top row) or *alg-3/4* males (bottom row) cultured at 20°C (left) or 25°C (center and right). Examples of membranous organelles (black arrowheads) and fibrous bodies (fb) are indicated. Representative nuclei of WT and *alg-3/4* spermatozoa are shown at right. Dotted lines emphasize the RNA halo surrounding the WT nucleus. White arrows label large tubule-like structures (visible in cross-section; Ward et al., 1981) adjacent to *alg-3/4* nuclei. See also Figure S1.

RNAs called 22G-RNAs (Gu et al., 2009). These 22G-RNAs are in turn loaded onto members of an expanded group of Worm-specific Argonaute (WAGO) proteins (Yigit et al., 2006), which silence gene expression transcriptionally and posttranscriptionally (Buckley et al., 2012; Gu et al., 2009). This form of RNA-induced epigenetic silencing (referred to as RNAe) is then stably transmitted via both the sperm and the egg, apparently indefinitely through subsequent generations (Shirayama et al., 2012).

A major question related to the mechanism by which PRG-1 surveys germline gene expression is how certain mRNAs are recognized as self and protected from silencing. The CSR-1 Argonaute is a candidate factor for mediating self-recognition. CSR-1 is related to WAGOs but engages RdRP-derived small RNAs antisense to most if not all germline-expressed mRNAs. Therefore, it is possible that targeting by CSR-1 prevents PRG-1 recognition of self mRNA. If this model is correct, then a mechanism must exist during gametogenesis to package a cache of CSR-1 22G-RNAs reflecting the state of gene expression during each phase of the germline life cycle.

In this study, we investigate the role of Argonaute small RNA pathways during spermatogenesis in *C. elegans*. Previous work identified ALG-3 and ALG-4 (ALG-3/4) as redundant AGO-clade Argonautes that promote male fertility (Conine et al., 2010; Han et al., 2009). ALG-3/4 engage a class of Dicer and RdRP-dependent small RNAs termed 26G-RNAs that are antisense to mRNAs expressed during spermatogenesis (Conine et al., 2010; Han et al., 2009; Pavelec et al., 2009). Here, we show that sperm transcripts that are targeted by ALG-3/4 26G-RNAs are also targeted by CSR-1 22G-RNAs in the male germline. We show that *alg-3/4* and *csr-1* mutant males exhibit identical temperature-sensitive sterile phenotypes that result from failed spermiogenesis. Both ALG-3/4 and CSR-1 are required for robust transcription of spermiogenic mRNAs, suggesting that ALG-3/4 and CSR-1 function in the same pathway. Consistent with this, CSR-1 associates with the chromatin of spermiogenic genes and localizes to chromatin at the periphery of sperm nuclei in an ALG-3/4-dependent manner.

ALG-3/4 and 26G-RNAs are absent or greatly reduced in mature sperm (Conine et al., 2010). However, we show that CSR-1 and associated 22G-RNAs antisense to ALG-3/4 targets are abundant in mature sperm. Surprisingly, sperm also contain CSR-1 small RNAs antisense to female-specific germline mRNAs. We show that heterozygous offspring of homozygous *alg-3/4* or *csr-1* males exhibit reduced fertility. Moreover, repeatedly backcrossing heterozygous hermaphrodites to homozygous mutant males results in a progressive loss of fertility (germline-mortal phenotype) that can be rescued by WT sperm. Taken together, these findings are consistent with a model in which ALG-3/4 and CSR-1 and their associated small RNAs provide an epigenetic memory of paternal gene expression, thereby ensuring the transgenerational continuity of a robust spermiogenic program.

RESULTS

Previously Identified *fer* Genes Function in the ALG-3/4 Pathway

The infertility phenotypes of *alg-3/4* mutant sperm are identical to those of temperature-sensitive fertilization-defective (*fer*) mutants isolated in genetic screens more than 30 years ago (Argon and Ward, 1980; Hirsh and Vanderslice, 1976). To date, most of the *fer* genes remain molecularly uncharacterized except for *fer-1*, which encodes a member of the Ferlin family of membrane proteins required for the fusion of intracellular vesicles during spermiogenesis (Washington and Ward, 2006).

The similarity of *alg-3/4* and *fer* mutant phenotypes extends to the ultrastructural level as assayed by electron microscopy (Figure 1; see Extended Results). For example, *alg-3/4* mutants, like the previously characterized *fer* mutants, arrest as round nonpolarized spermatids in which sperm-specific organelles fail to undergo a series of stereotypic fusion events and structural reorganizations that drive pseudopod formation. Mutant spermatids also exhibit a missing or abnormal perinuclear RNA halo (Figure 1; Ward et al., 1981). Given the striking similarities between the *fer* and *alg-3/4* mutant phenotypes, we asked whether the *fer* genes might function in the ALG-3/4 pathway.

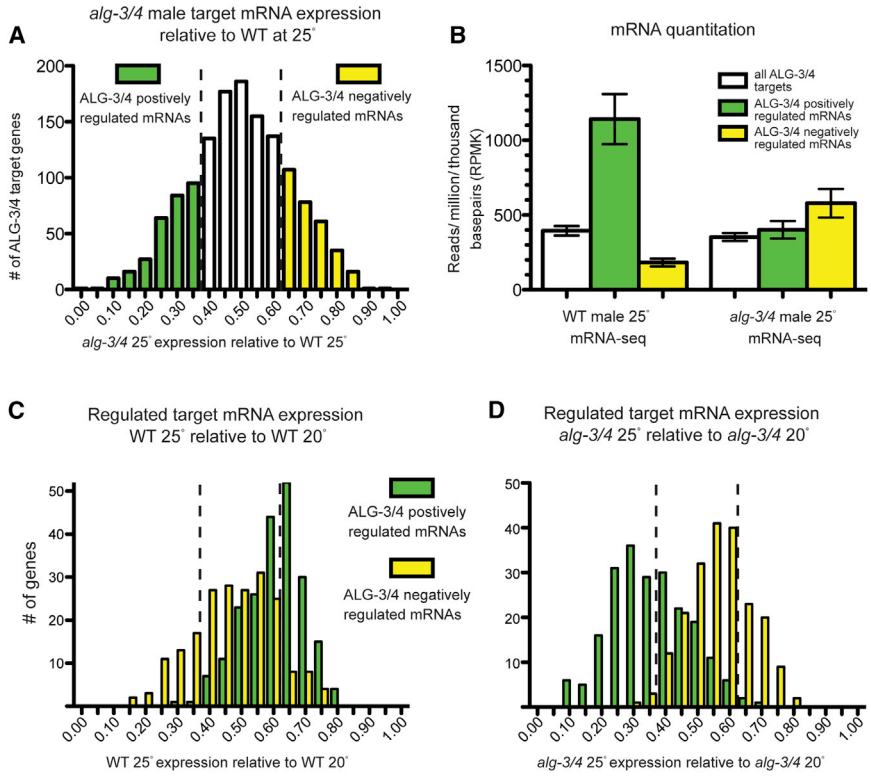

Figure 2. ALG-3/4 Positively and Negatively Regulated Hundreds of Target mRNAs

(A) Histogram illustrating the enrichment or depletion of ALG-3/4 target mRNAs in *alg-3/4* mutants relative to WT at 25°C. Dotted lines indicate a 2-fold change, values approaching 1 indicate enrichment (ALG-3/4 negatively regulated mRNAs), and values approaching 0 indicate depletion (ALG-3/4 positively regulated mRNAs). In (A)–(D), colored bars indicate ALG-3/4 targets positively regulated (green) or negatively regulated (yellow) more than 2-fold. Enrichment was calculated as the reads per million (RPM) ratio of *alg-3/4* / (*alg-3/4* + WT).

(B) Bar graphs showing the average RPM per kilobase (RPMK) for ALG-3/4 regulated targets in WT or *alg-3/4* mutant at 25°C.

(C and D) Histogram illustrating the enrichment of positively or negatively regulated ALG-3/4 target mRNAs in WT (C) or *alg-3/4* (D) males at 25°C relative to 20°C. Enrichment was calculated as the RPM ratio of 25°C/(25°C + 20°C).

See also Figures S2 and S3 and Tables S1 and S2.

This analysis revealed that *fer-2*, *fer-3*, *fer-4*, *fer-6*, and *fer-15* exhibit defects in the production of ALG-3/4 pathway 26G-RNAs (Figure S1A available online). Furthermore, we found that *fer-3(hc3)* and *fer-15(b26)* exhibit an Eri phenotype (Figure S1B) and, like other *eri* mutants, are required for ERGO-1 pathway 26G-RNAs (Figure S1A). Indeed, *fer-3* and *fer-15* mutations map nearby the ERI-pathway genes *eri-3* and *rrf-3*, respectively (Ward et al., 1981). *fer-3(hc3)* failed to complement the Fer and Eri phenotypes of *eri-3(tm1361)* (Figure S1B). Consistent with this finding and the partial loss of male-specific 26G-RNAs, we identified a nucleotide substitution in exon 3 of *eri-3* that is predicted to result in a serine-to-proline missense mutation at amino acid 69 (Figure S1C). *fer-15(b26)* failed to complement the Fer and Eri phenotypes of *rrf-3(pk1426)*, and we identified a 223 bp deletion that removes exon 6 of *rrf-3* and is predicted to shift the reading frame and introduce a premature termination codon (Figure S1C). *fer-2*, *fer-4*, and *fer-6* mutants were not Eri, and their molecular identities remain to be determined. Taken together, our findings indicate that several previously isolated *fer* mutants define genes that function in the ALG-3/4-26G-RNA pathway.

Target Regulation by ALG-3/4 and 26G-RNAs

Our previous deep-sequencing studies identified 397 genes as high-confidence targets of ALG-3/4-dependent 26G-RNAs using a 10 reads-per-million (RPM) cutoff (Conine et al., 2010). To identify the full repertoire of ALG-3/4 targets, we cloned and deep sequenced small RNAs isolated from *alg-3/4* males and wild-type (WT) males cultured at both 20°C and 25°C. In total, we identified 1,497 genes targeted by 26G-RNAs in WT males at a density of at least 5 RPM. We found that 94% (1,408) of these genes exhibited a >2-fold reduction in 26G-RNAs in *alg-3/4* mutants and were thus designated as ALG-3/4 target genes (Table S1). The remaining 6% of genes targeted by 26G-RNAs that were unaffected in *alg-3/4* mutants are likely to be ERGO-1-dependent 26G-RNA targets (Vasale et al., 2010). The expanded list of 1,408 ALG-3/4 26G-RNA targets accounts for 63% (617/970) of genes with sperm-specific expression (Reinke et al., 2004).

Many ALG-3/4 targets are required for spermiogenesis and are involved in pseudopod formation and sperm motility. For example, these targets include genes that encode MSPs and MSP-related proteins (Burke and Ward, 1983), as well as factors required for sperm motility (Buttery et al., 2003). Because the activities of ALG-3/4 and of many of their target genes are required for spermiogenesis, it therefore seemed unlikely that ALG-3/4 directs the silencing of these targets. To determine how ALG-3/4 and associated 26G-RNAs regulate their targets, we performed a combination of mRNA deep sequencing (mRNA-seq) and proteomics on WT and *alg-3/4* mutant males grown at 20°C and 25°C (Figures 2A and S2A). Findings from this analysis, which are detailed in the Supplemental Information, suggest that ALG-3/4 promote the expression of many targets and do so by increasing corresponding mRNA levels at elevated temperatures. We found that approximately 214 target mRNAs were positively regulated by 2-fold or more (decreased by 2-fold or more in the mutant), 204 were negatively regulated by 2-fold or more, and 991 target mRNAs did not change (Figure 2A and Table S1). Strikingly, we found that positively regulated mRNAs were much more abundant in WT males than were nonregulated (4-fold lower) or negatively regulated (6-fold lower) mRNAs (Figure 2B). This enrichment of positively regulated

mRNAs was completely dependent on ALG-3/4 activity (was abolished in *alg-3/4* mutants, Figure 2B). Our proteomic analysis revealed 122 proteins that decreased by at least 1.5-fold in *alg-3/4* mutants relative to WT and 43 that increased (Figure S2A and Table S2). For each protein identified in our proteomic analysis, we compared the change in protein level in *alg-3/4* males at 25°C to the change in mRNA (Figures S2B and S2E). For most ALG-3/4-dependent positively regulated proteins (81/122, 66%), the decrease in protein level in the *alg-3/4* mutant could be explained by a reduction in the corresponding mRNA. By contrast, for 33% (14/43) of ALG-3/4 negatively regulated proteins, we found that the increase in protein could be attributed to changes in corresponding mRNAs. These data indicate that the ALG-3/4 pathway promotes the expression of many of its targets and does so by increasing their mRNA levels.

In *alg-3/4* mutants, sperm defects are much more severe at high temperature (Conine et al., 2010). We therefore wished to know how ALG-3/4 target mRNA levels changed with temperature in both the WT and *alg-3/4* mutant strains. We found that, in WT males, positively regulated mRNAs increased at 25°C relative to 20°C, whereas negatively regulated mRNAs tended to decrease at 25°C (Figure 2C). The converse was true for *alg-3/4* mutant males: positively regulated mRNAs decreased dramatically at 25°C compared to 20°C, whereas negatively regulated targets increased, albeit less dramatically (Figure 2D). Similar analyses of our proteomic data also corroborate these findings (Figures S2C and S2D). The described changes in transcript levels by mRNA-seq were confirmed using quantitative RT-PCR (qRT-PCR) (Figure S3). These data support the existence of at least two distinct classes of ALG-3/4 target genes: one that is dramatically upregulated by ALG-3/4 at elevated temperature, and one that is moderately downregulated by ALG-3/4 at elevated temperature.

ALG-3/4 positively regulated targets are clearly genes required for spermiogenesis and motility, including many of the MSP and MSP-related genes involved in pseudopod formation, as well as the PP1 phosphatases encoded by *gsp-3/4*, which are required for multiple aspects of *C. elegans* sperm development and when mutated exhibit temperature-sensitive (TS) sperm defects similar to *alg-3/4* (Wu et al., 2012). ALG-3/4 negatively regulated targets include genes associated with mitochondrial function (electron transport chain and cellular respiration), but a correlation between reproductive genes and negatively regulated ALG-3/4 targets was not observed (Tables S1 and S2).

To confirm that ALG-3/4 promotes the expression of target genes in the germline, we used immunofluorescence (IF) assays to detect MSP and GSP-3 proteins and fluorescence in situ hybridization (FISH) to detect *msp* transcripts. Interestingly, IF of MSP and GSP-3, two positively regulated targets, suggested that these proteins were only slightly reduced in *alg-3/4* germlines during spermatogenesis and in haploid spermatids at 20°C compared to WT (Figure 3A). At 25°C, however, MSP and GSP-3 were severely reduced throughout the spermatogenic germline of *alg-3/4* males compared to WT and failed to accumulate in spermatids (Figure 3A). Although GSP-3 protein was depleted overall, we found that it also accumulated abnormally in the nuclei of *alg-3/4* mutants, particularly at 25°C (Figure 3A). In addition, we observed more nuclei undergoing chromatin condensation in *alg-3/4* males compared to WT males (see below). Examining spermatids released from the testes of *alg-3/4* mutants raised at 25°C and activated to undergo spermiogenesis in vitro revealed that 12% of *alg-3/4* spermatozoa accumulate near WT levels of MSP and GSP-3. Unlike WT spermatozoa, however, these *alg-3/4* spermatozoa never formed pseudopods of normal morphology or polarity, with MSP and GSP-3 localized to the leading edge of the pseudopod (Figure 3B). Instead, we observed that (1) MSP and GSP-3 remained in large punctae that resemble sperm organelles called fibrous bodies (FBs) (5%), (2) MSP localized to the cortex and GSP-3 to the cytoplasm of the spermatid but lacked polarity (3%), or (3) GSP-3 remained in the cytoplasm and spermatids formed a multibranched, spikey pseudopod containing MSP (4%). Consistent with our mRNA-seq and qRT-PCR data, FISH revealed that *msp* mRNA was indeed reduced in the spermatogenic germline of *alg-3/4* males compared to WT males (Figure 3C). This reduction was more pronounced at 25°C, with very little signal detected in *alg-3/4* male germlines, consistent with the temperature-dependent regulation of expression (Figure 3C).

ALG-3/4 Promotes the Transcription of Target Genes

Our findings suggest that ALG-3/4 positively regulates targets at the level of the mRNA. We therefore sought to determine whether ALG-3/4 promotes the transcription of positively regulated targets. Using RNA polymerase II (Pol II) chromatin immunoprecipitation (ChIP) followed by quantitative PCR, we found that Pol II occupancy of positively regulated ALG-3/4 targets decreased 1.5- to 3-fold in *alg-3/4* males compared to WT males cultured at 20°C. Notably, Pol II occupancy was reduced 3- to 7-fold in *alg-3/4* males grown at 25°C (Figure 4A). Consistent with the reduced Pol II occupancy in *alg-3/4* males, the pre-mRNAs of positively regulated targets were also decreased in *alg-3/4* and *fer-15/rrf-3* males by 2- to 4-fold at 20°C and by 4- to 8-fold at 25°C. These findings suggest that both the Argonaute (ALG-3/4) and RdRP (FER-15/RRF-3) promote the transcription of positively regulated targets (Figure 4B). Pol II occupancy of *spe-12* and *col-122* (two control genes expressed in male germline and somatic tissues [respectively], but not targeted by ALG-3/4 26G-RNAs) was not dependent on *alg-3/4* or temperature (Figure 4A).

Curiously, Pol II occupancy of the negatively regulated gene *ssp-16* was reduced by 2- and 3-fold in *alg-3/4* males at 20°C and 25°C, respectively, relative to WT levels (Figure 4A). Pol II occupancy of a second negatively regulated target *f36h12.4* was unchanged at 20°C and reduced nearly 2-fold at 25°C compared to WT levels (Figure 4A). The expression of the *f36h12.4* pre-mRNA mirrored these findings. Each of the five negatively regulated targets that we examined showed a similar reduction in pre-mRNA at 25°C (Figure 4B). These results, therefore, suggest that negatively regulated ALG-3/4 targets are silenced at a posttranscriptional level.

Because the WAGO 22G-RNA pathway is required for silencing (Gu et al., 2009), we tested whether the WAGO pathway is required to silence negatively regulated ALG-3/4 targets at a posttranscriptional level. Indeed, we found that the mRNA levels of several negatively regulated targets were increased

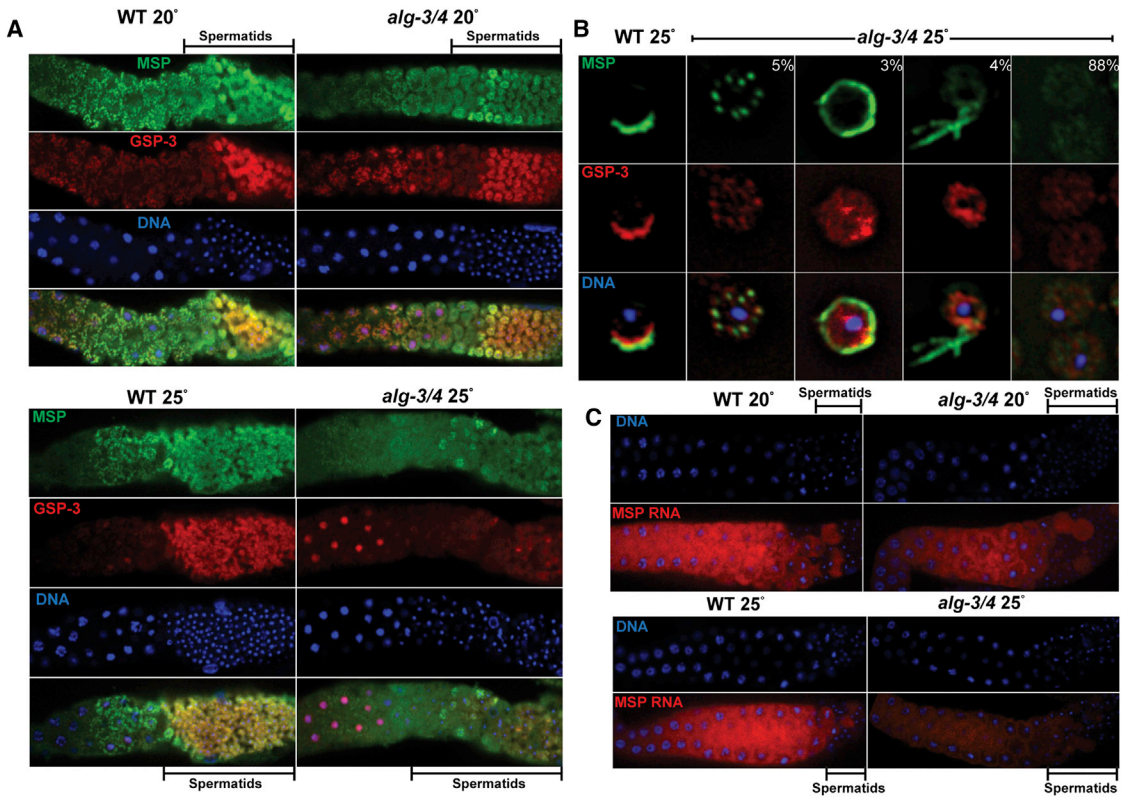

Figure 3. ALG-3/4 Positively Regulate Genes Required for Spermiogenesis

(A–C) Confocal images of WT and *alg-3/4* mutant gonads (A and C) and activated spermatocytes (B). Each column of photographs represent a single specimen imaged with different fluorescence channels (as indicated). A merged image is shown at the bottom. The genotype and temperature at which spermatogenesis occurred are indicated. DNA was visualized by DAPI staining (blue). In (A) and (B), the sperm proteins MSP (green) and GSP-3 (red) are visualized by immunofluorescence. In (B), the percentage of WT and *alg-3/4* spermatozoa that exhibit the staining pattern shown is indicated. In (C), *msp* mRNA is visualized by fluorescence in situ hybridization (FISH).

in males lacking *rde-3* or deleted for all 12 WAGOs (MAGO-12; Figure S4). These increased levels were similar to those observed in *alg-3/4* males (Conine et al., 2010). Strikingly, the pre-mRNA levels of these negatively regulated targets remained unchanged in *rde-3* or MAGO-12 males. Thus, as previously hypothesized (Conine et al., 2010), ALG-3/4 negatively regulates a subset of its targets at a posttranscriptional level via the WAGO pathway.

To examine the temporal and spatial regulation of transcription in the male germline by ALG-3/4, we stained male germlines with an antibody that recognizes elongating Pol II (Ahn et al., 2004). In WT germlines at 25°C, elongating Pol II was detected at the periphery of condensing spermatocyte nuclei and in small discrete foci in spermatids (Figure 4C). By contrast, in *alg-3/4* germlines at 25°C, elongating Pol II disappeared from spermatocyte nuclei at the onset of the condensation process (Figure 4C) but was detected later in spermatogenesis throughout the nucleus in spermatocytes, not just at the nuclear periphery (Figure 4C). We next examined a histone modification associated with actively transcribed chromatin (histone H3 dimethylated on lysine 4 [H3K4me2]; Kelly et al., 2002). This analysis revealed H3K4me2 localization throughout the nucleus in WT spermatocytes at 25°C. However, H3K4me2 was dramatically reduced in *alg-3/4* spermatocytes and was present only in small patches of chromatin (Figure 4D).

CSR-1 Acts in the ALG-3/4 Pathway to Promote Sperm Development

Previous work suggested that the Argonaute CSR-1 and its 22G-RNA cofactors target but do not silence germline-expressed genes (Claycomb et al., 2009), and recent work suggests that CSR-1 promotes germline transgene expression (Seth et al., 2013). Homozygous *csr-1(tm892)* mutant hermaphrodites are essentially sterile but produce a few embryos that die due to chromosome segregation defects (Yigit et al., 2006; Claycomb et al., 2009). Although *csr-1* males were sterile at 25°C, we were surprised to find that they were ~50% fertile relative to WT males at 20°C (Figure 5A). This temperature-dependent sterility was similar to that observed for *alg-3/4*. Indeed, like *alg-3/4* mutant spermatids, *csr-1* spermatids failed to complete spermiogenesis at 25°C and arrested as either round spermatids or spermatids with nonmotile or spiky pseudopods (Figure 5A).

Consistent with the possibility that CSR-1 functions in the same pathway as ALG-3/4, we found that triple *csr-1 alg-3; alg-4* mutant males were completely sterile at 25°C with defects in spermiogenesis almost identical to those observed in the *csr-1*

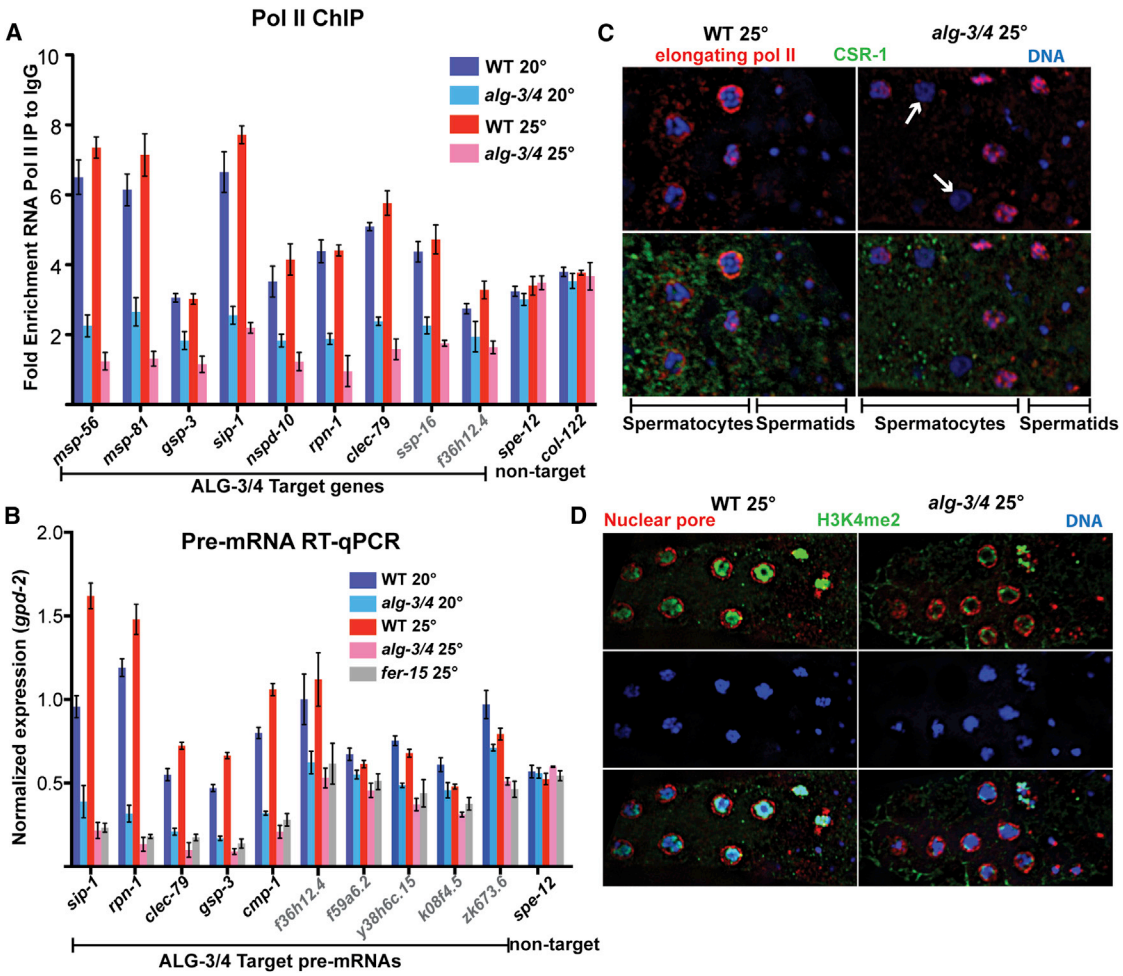

Figure 4. ALG-3/4 Promote Transcription in Condensing Meiotic Nuclei

(A) Quantitative PCR analysis of RNA Pol II ChIP at ALG-3/4 target genes in WT and *alg-3/4* mutants at 20°C and 25°C, normalized to an intergenic region not occupied by Pol II. Data are represented as mean ± SEM. ALG-3/4 negatively regulated targets are labeled in gray.

(B) qRT-PCR analysis of ALG-3/4 target pre-mRNAs. Data are normalized to the nontarget *gpd-2* pre-mRNA and represented as mean ± SEM.

(C and D) Confocal IF images of dissected WT (left) or *alg-3/4* (right) spermatogenic germlines at 25°C stained with antibodies against (C) elongating RNA Pol II (red) and CSR-1 (green) or (D) antibodies against H3K4me2 (green) and nuclear pore proteins (red). White arrows denote spermatocyte nuclei lacking Pol II staining. DNA was stained with DAPI (blue).

See also Figure S4.

single and *alg-3/4* double mutants, respectively (Figure 5A; Conine et al., 2010). At 20°C *csr-1 alg-3; alg-4* males exhibited fertility defects similar to, but slightly more severe, than *csr-1* or *alg-3/4* males (Figure 5A). Furthermore, *csr-1* males grown at 25°C exhibited defects in elongating Pol II and H3K4me2 localization in the spermatogenic germline that were indistinguishable from phenotypes observed in *alg-3/4* males at 25°C (Figure S5A). Taken together, these findings suggest that CSR-1 functions along with ALG-3/4 to promote a chromosomal environment compatible with transcription. Perhaps consistent with this idea, we observed an increase in the number of spermatocytes undergoing nuclear condensation in both *alg-3/4* and *csr-1* males. The increase was moderate at 20°C (1.2- to 1.4-fold) but enhanced at 25°C, with both *alg-3/4* and *csr-1* mutants showing a nearly 2-fold increase in the number of condensing nuclei relative to WT (Figure S5B). These observations suggest that spermatocyte nuclei begin to condense prematurely or fail to complete condensation appropriately in *alg-3/4* and *csr-1* mutants.

In the hermaphrodite germline, CSR-1 localizes to perinuclear P-granules and to condensed chromatin in oocytes (Claycomb et al., 2009). In addition, CSR-1 was identified in a proteomic study as a protein associated with sperm chromatin (Chu et al., 2006). To examine the expression pattern and localization of CSR-1 during male gametogenesis, we performed immunofluorescence using an antibody that recognizes endogenous CSR-1 (Claycomb et al., 2009). CSR-1 was associated with P-granules throughout the syncytial male germline and into differentiating spermatocytes, where P-granules disperse and disappear. In developing gametes, we found that CSR-1

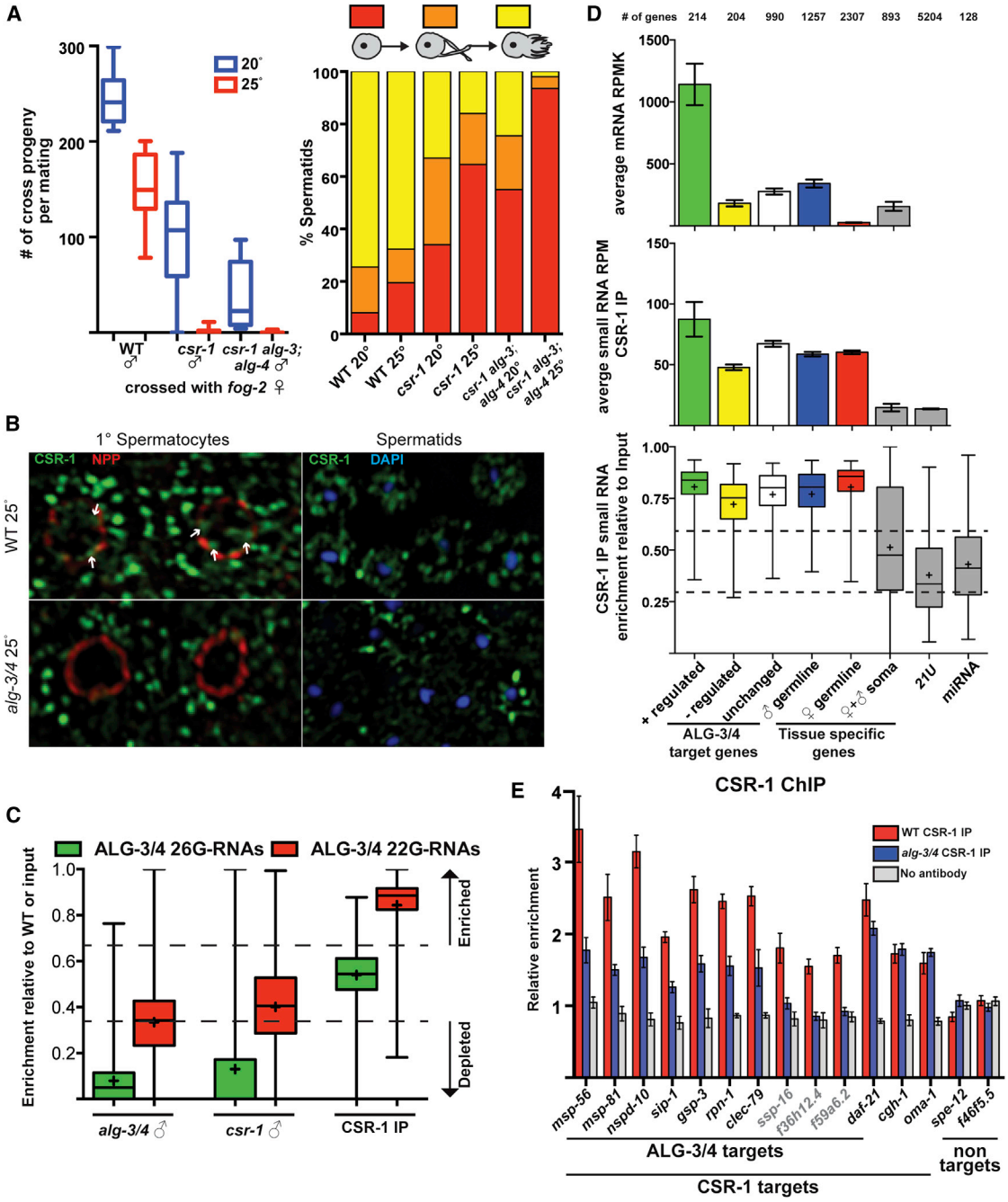

Figure 5. CSR-1 Associates with Both Male- and Female-Specific Small RNAs in Males and Positively Regulates Spermiogenic Gene Expression

(A) Left: fertility of WT, *csr-1*, or *csr-1 alg-3; alg-4* males at 20°C or 25°C measured in crosses with *fog-2* females. Box and whisker plots represent a range of cross progeny from at least 15 independent crosses for each genotype. Right: in vitro activation of spermatids isolated from *csr-1*, *csr-1 alg-3; alg-4*, or WT males grown at 20°C or 25°C. Bar graphs show the percent of spermatids that fail to activate (red), partially activate and form spikey projections (orange), or fully activate and form a pseudopod (yellow) (n > 300).

(B) Confocal IF images of primary (1°) spermatocytes (left) or spermatids (right) in dissected *alg-3/4* or WT germlines stained with antibodies against CSR-1 (green) and a nuclear pore protein (red). DNA was stained with DAPI (blue). White arrows denote chromatin domains where CSR-1 localizes.

(C) Box and whisker plots indicate depletion of 26G-RNAs and 22G-RNAs antisense to ALG-3/4 targets in *alg-3/4* and *csr-1* males at 25°C. Box and whisker plots to the right indicate enrichment of 22G-RNA and lack of enrichment of 26G-RNAs antisense to ALG-3/4 targets in the CSR-1 IP.

(D) Analysis of mRNA expression and CSR-1 small RNA levels in WT males. Categories of gene expression are indicated below the bottom graph. ALG-3/4 targets as defined in Figure 1: positively regulated (green), negatively regulated (yellow), and unchanged (white). Male-germline-specific genes (blue) include many

(legend continued on next page)

localized to large cytoplasmic foci and in discrete chromatin domains of spermatocytes undergoing nuclear condensation as well as in haploid spermatids (Figure 5B). In *alg-3/4* mutants cultured at 25°C, CSR-1 was present in large cytoplasmic foci in spermatocytes undergoing nuclear condensation but was largely absent from chromatin. Notably, in haploid spermatids from *alg-3/4* males, we observed fewer CSR-1 cytoplasmic and nuclear foci than in haploid spermatids from WT males (Figure 5B). Taken together, these findings suggest that CSR-1 functions with ALG-3/4 to promote gene expression in developing spermatocytes.

CSR-1 22G-RNAs Target Genes Also Targeted by ALG-3/4 26G-RNAs

The similarities between the cellular and developmental phenotypes of *alg-3/4* and *csr-1* males are consistent with the possibility that ALG-3/4 and CSR-1 function in the same small RNA pathway. To determine whether CSR-1 is required for the expression of small RNAs antisense to ALG-3/4 targets, we cloned and deep sequenced small RNAs from *csr-1* males grown at 25°C. Remarkably, we found that ALG-3/4-dependent 26G-RNAs, regardless of class (i.e., antisense to positively or negatively regulated targets), were strongly depleted in *csr-1* males. Indeed, this depletion was to a level resembling that of *alg-3/4* mutant males (Figure 5C). On the other hand, 22G-RNAs were only slightly depleted in *alg-3/4* and *csr-1* males (Figure 5C). A similar minor reduction of 22G-RNAs was observed previously when small RNAs were cloned from *csr-1* hermaphrodites (Claycomb et al., 2009). While these findings are consistent with the idea that ALG-3/4 and CSR-1 function in the same pathway, they also suggest that the pathway may not be linear (see Discussion).

To further explore the idea that CSR-1 and ALG-3/4 share targets, we cloned and deep sequenced CSR-1-associated 22G-RNAs. To do this, we performed CSR-1-immunoprecipitation (IP) followed by small RNA deep sequencing from males expressing a rescuing FLAG::CSR-1 transgene and grown at 25°C. We found that CSR-1 IP enriched small RNAs targeting 5,575 genes, including 90% (3,775/4,190) of the genes previously identified as CSR-1 targets in the hermaphrodite (Claycomb et al., 2009). Surprisingly, we found that small RNAs targeting many female-specific genes were also enriched (Figure 5D; see Extended Results). As expected, CSR-1 IP did not enrich microRNAs or 21U-RNAs, nor did it enrich 22G-RNAs previously identified as WAGO-1-associated in hermaphrodites (Claycomb et al., 2009; Gu et al., 2009). We also recovered small RNAs that target ~1,800 genes (Table S3) not previously identified as CSR-1 targets, including most annotated male-germline-expressed genes. Notably, using a 2-fold cutoff, FLAG::CSR-1 IP enriched for small RNAs antisense to 82% (1,156/1,408) of all ALG-3/4 targets defined in this study (Figure 5D), including 88% (188/214) of ALG-3/4 positively regulated genes, 83% (821/991) of nonregulated genes and 72% (147/204) of ALG-3/4 negatively regulated genes (Figure 5D). Thus, just as CSR-1 is required for all ALG-3/4 26G-RNAs, these findings indicate that CSR-1 associates with 22G-RNAs targeting most and perhaps all ALG-3/4 targets.

CSR-1 Promotes the Expression of ALG-3/4 Targets

CSR-1 was previously shown to associate with the chromatin of its 22G-RNA target genes in hermaphrodites (Claycomb et al., 2009). To ask whether CSR-1 associates with the chromatin of genes targeted by ALG-3/4 in males, we performed CSR-1 ChIP on WT and *alg-3/4* male populations grown at 25°C. We found that in WT males, CSR-1 ChIP enriched all of the ALG-3/4 targets assayed, including both positively and negatively regulated targets, by 1.5- to 3-fold relative to a no-antibody control (Figure 5E). This enrichment was not detected in *alg-3/4* mutant animals (Figure 5E). CSR-1 ChIP from males also enriched several genes that were previously identified as CSR-1 targets in hermaphrodites, including *daf-21*, *cgh-1*, and *oma-1* (Claycomb et al., 2009). The latter two, *cgh-1* and *oma-1*, were only weakly expressed in males (data not shown) and were not ALG-3/4 targets. As expected, we found that the association of CSR-1 with these two loci was independent of ALG-3/4 (Figure 5E). CSR-1 ChIP did not enrich *spe-12* or *f46f5.5*, genes that are not targeted by ALG-3/4- or CSR-1-associated small RNAs (Figure 5E). Using qRT-PCR, we found that the mRNA and pre-mRNA levels of positively regulated ALG-3/4 targets were reduced by similar amounts in *csr-1* males (see Figure 6C below). By contrast, we found that mRNA levels of ALG-3/4 negatively regulated targets were unchanged in *csr-1* mutant males at 25°C (Figure S3), while pre-mRNA levels decreased (see Figure 6C below). This latter finding (that pre-mRNA levels decrease for ALG-3/4 negatively regulated targets) was also observed, paradoxically, in *alg-3/4* mutant males (Figure 4B). Taken together, these findings indicate that targets positively regulated by ALG-3/4 are also positively regulated by CSR-1 and suggest that ALG-3/4 and CSR-1 promote the expression of their targets at a transcriptional level, including a subset of ALG-3/4 targets whose net expression is negatively regulated due to posttranscriptional silencing.

CSR-1 and ALG-3/4 Provide a Paternal Memory of Past Gene Expression

The ALG-3/4 proteins are present during spermatogenesis but are eliminated from maturing spermatids (Conine et al., 2010). The CSR-1 protein, however, is abundant in mature sperm

ALG-3/4 targets. Female-germline specific genes (red) are not targeted by ALG-3/4. Soma-specific mRNAs and 21U-RNAs are control sequences not enriched by CSR-1 IP. The number of genes in each category is indicated above the graphs. Top graph: mRNA expression as monitored by RNA-Seq in reads per million per kilobase (RPMK). Middle graph: small RNA levels in reads per million (RPM) per gene. Bottom graph: box and whisker plot indicating the enrichment or depletion in CSR-1 IP of small RNAs antisense to genes. Enrichment was calculated as the RPM ratio of FLAG::CSR-1 IP/(FLAG::CSR-1 IP + input). Dotted lines indicate 2-fold enrichment (upper) or depletion (lower). The plus sign (+) indicates the average enrichment value for all genes in the category.

(E) qPCR analysis of FLAG::CSR-1 ChIP at genes targeted by ALG-3/4, CSR-1, or neither. ALG-3/4 negatively regulated targets are indicated in gray text. Data were normalized to *y47h10a.3*, which is not targeted by ALG-3/4 or CSR-1. Data are represented as mean ± SEM.

See also Figures S3 and S5 and Table S3.

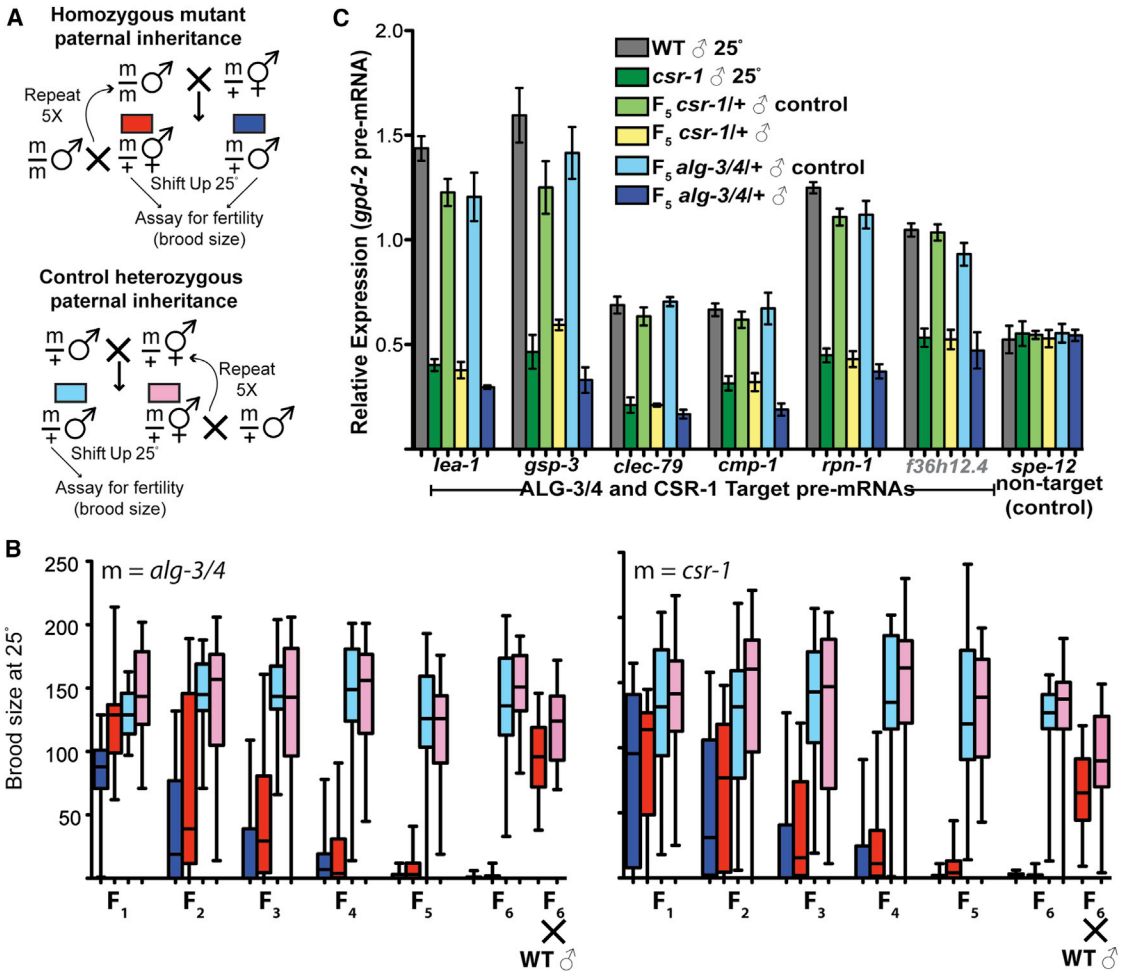

Figure 6. ALG-3/4 and CSR-1 Provide a Paternal Memory of Germline Gene Expression

(A) Schematic of crosses to assay paternal inheritance of gene expression and sperm function. m indicates either *csr-1* or *alg-3/4* allele.

(B) Repeated mating with *alg-3/4* and *csr-1* males induces a progressive dominant germline-mortal phenotype. Box and whisker plots indicate the brood sizes of heterozygous hermaphrodite (red/pink) and male (blue/aqua) cross progeny of homozygous mutant fathers (red and blue) or control heterozygous hermaphrodites and males (pink and aqua, respectively) determined in successive generations of mating to homozygous (blue) or heterozygous (aqua) *alg-3/4* (left) or *csr-1* (right) mutant males. Fertility of male cross progeny was assayed by mating to *fog-2* females.

(C) qRT-PCR analysis of pre-mRNA levels in male cross progeny (as indicated by color). Data are normalized to *gpd-2* pre-mRNA and represented as mean ± SEM. CSR-1 and ALG-3/4 target mRNAs, and a nontarget mRNA were assayed (as indicated). An ALG-3/4 negatively regulated target is indicated in gray text.

(Figure 5B). We therefore wondered if ALG-3/4 and CSR-1 might function together to pass a memory of male-specific gene expression from one generation to the next via CSR-1. To test this idea, we first analyzed the fertility of *alg-3/4* and *csr-1* heterozygous hermaphrodites (F_1) cultured at 25°C. We then mated heterozygous hermaphrodites to homozygous *alg-3/4* or *csr-1* males, respectively, at the permissive temperature to obtain F_2 heterozygous hermaphrodites. In this and subsequent generations, the resulting heterozygous offspring were cultured at 25°C to assay their fertility before being mated to homozygous males at 20°C (Figure 6A). In parallel, as a control, we mated heterozygous hermaphrodites to heterozygous males to obtain heterozygous offspring (Figure 6A). Thus, the maternal genotype was always heterozygous throughout this analysis, whereas the paternal genotype was either homozygous (experimental series) or heterozygous (control series). Remarkably, we found that heterozygous offspring (hermaphrodites or males) derived from homozygous *alg-3/4* or *csr-1* males became progressively less fertile with each generation at 25°C (Figure 6B). By the sixth generation (F_6), the heterozygous offspring of *alg-3/4* or *csr-1* homozygous males were completely sterile. The sterility of F_6 heterozygous hermaphrodites could be rescued by mating to WT males, indicating that the sterility was due to a sperm defect. In the control series, on the other hand, the heterozygous offspring of heterozygous males maintained a consistent level of fertility throughout the course of the experiment. Importantly, the impaired fertility of heterozygous *alg-3/4* and *csr-1* offspring correlated with declining pre-mRNA expression levels of ALG-3/4 targets. By the F_5 generation, relative to either control heterozygous males or WT males, the heterozygous male offspring of homozygous males exhibited

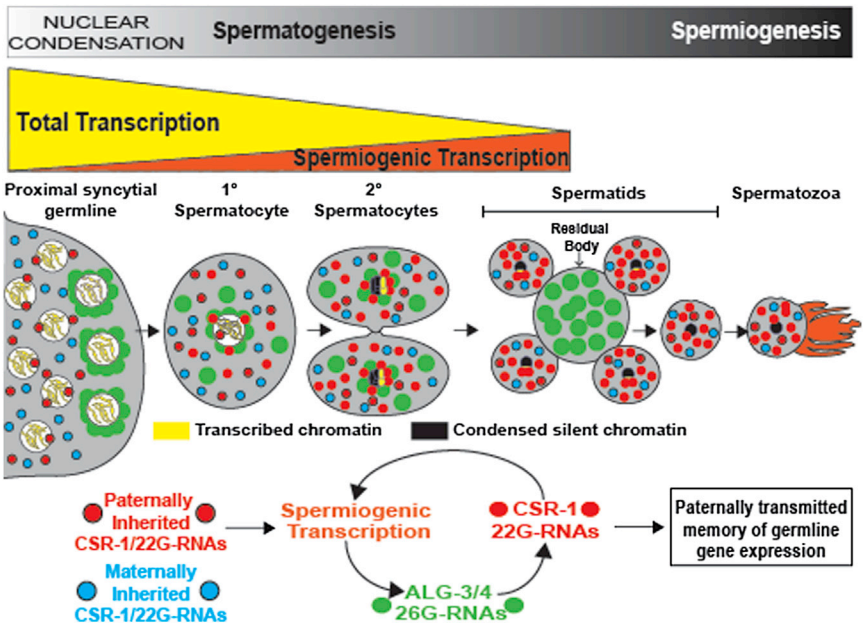

Figure 7. Model

ALG-3/4 and CSR-1 and their small RNA cofactors promote the transcription of spermiogenic genes and provide a memory of past germline gene expression. Black dots in spermatids represent areas of condensed silent chromatin; yellow areas indicate transcriptionally active chromatin. See Discussion for details.

a reduction in pre-mRNA similar to *alg-3/4* or *csr-1* males at 25°C (Figure 6C). Thus, ALG-3/4 and CSR-1 promote a paternal epigenetic memory of ALG-3/4 target gene expression.

DISCUSSION

A Small RNA Feed-Forward Loop Transmits a Paternal Epigenetic Memory of Past Gene Expression

During male gametogenesis, germ cells proceed through meiosis and undergo dramatic changes in cellular morphology to produce haploid spermatids containing highly compacted, transcriptionally inert chromatin (Ward et al., 1981). The completion of this process and the subsequent transformation of spermatids into polarized motile spermatozoa capable of fertilization depend on the proper execution of an extensive gene-expression program involving thousands of genes. Here, we have shown that the Argonautes ALG-3/4 and CSR-1 are required during this process to promote robust spermatogenic gene expression. Although ALG-3/4 is absent from mature sperm (Conine et al., 2010), we have shown that CSR-1 is abundant in mature sperm. The propagation of strains lacking CSR-1 or ALG-3/4 activities in the paternal lineage caused a progressive loss of fertility (a germline-mortal phenotype), in which even heterozygous descendants, with a WT copy of the respective locus, exhibited complete sperm-specific sterility when assayed at 25°C. The observed infertility involved an arrest as round spermatids with decreased transcription of ALG-3/4 targets, a phenotype identical to that observed in *alg-3/4* and *csr-1* homozygous mutants. These findings suggest that ALG-3/4 and CSR-1 are not only required to promote spermatogenic gene expression but also act together to transmit an epigenetic memory of paternal gene expression via the sperm.

How might this work? Paternal CSR-1 22G-RNAs delivered via the sperm could enter the zygotic germline (see model, Figure 7). Later, when spermatogenesis initiates in hermaphrodites and males, CSR-1 targeting could recruit the RdRP-containing ERI complex (Duchaine et al., 2006; Pavelec et al., 2009) to initiate the production of 26G-RNAs that are loaded onto ALG-3/4. In a feed-forward mode, ALG-3/4 could then target cognate transcripts to recruit the EGO-1 RdRP complex to reamplify CSR-1 22G-RNAs (Claycomb et al., 2009; Conine et al., 2010; Gu et al., 2009). While the initial biogenesis of ALG-3/4 and CSR-1 small RNAs likely requires some template mRNA destruction, the net result of this amplification cycle appears to be increased mRNA levels, perhaps due to feedback on transcription. During spermatogenesis, CSR-1 and its 22G-RNA cofactors might promote gene expression by engaging nascent transcripts on the chromatin of its target genes. For example, CSR-1 could recruit factors that help maintain a transcriptionally active state during spermatogenesis and nuclear condensation, ensuring that spermatids obtain the appropriate level of gene products required for spermiogenesis. Finally, CSR-1/small RNA complexes could once again become incorporated into mature sperm, thus poised to reinitiate the cycle in the next generation (Figure 7).

A Protective Role for piRNAs across Phyla

In many animals, sperm development is inherently temperature sensitive (Rockett et al., 2001). The effects of elevated temperature during sperm development can also be epigenetically transmitted, causing developmental defects in mammalian embryos, including decreased embryonic mass and increased mortality (Jannes et al., 1998; Setchell et al., 1988). However, the molecular mechanism behind the temperature sensitivity of sperm development remains unclear.

Our findings indicate that the gene-expression programs required for spermatogenesis in *C. elegans* are sensitive to temperature. In WT males, the expression of many spermiogenesis genes was higher at 25°C than at 20°C. We have shown that ALG-3/4 and CSR-1 are required to initiate and maintain the activation of spermiogenesis genes at elevated temperatures. Failure to maintain spermiogenic gene expression in *alg-3/4* and *csr-1* mutants correlates with dramatic defects in spermatid activation and infertility in both mutant strains at elevated temperature. Thus, the ALG-3/4 and CSR-1 pathways appear to act as enhancers of gene expression that buffer the effects of temperature on sperm development.

In WT animals, the process of spermatogenesis accelerates by more than 25% at 25°C relative to 20°C, which in turn demands a similar increase in the expression of gene products that support spermiogenesis. Thus, increased gene expression is required in a setting where the rapid onset of meiosis and subsequent chromatin condensation would be expected to shut down transcription. Our findings suggest that the ALG-3/4 and CSR-1 pathways act together to selectively maintain transcriptionally active chromatin at spermiogenesis genes during meiotic nuclear condensation while packaging other regions of the genome not essential for spermiogenesis into transcriptionally inactive chromatin. This would create a burst of transcription of spermiogenesis genes near the end of spermatogenesis, as seen in mammals (Sassone-Corsi, 2002), when chromatin begins to condense in 1° spermatocytes (Shakes et al., 2009).

Interestingly, mice deficient for the PIWI homolog MIWI display spermatogenic arrest at the round spermatid stage (Deng and Lin, 2002), a phenotype similar to that of *alg-3/4* and *csr-1* mutant sperm. MIWI associates with pachytene piRNAs, ~29–31 nt small RNAs derived from large piRNA genes within nonrepetitive genomic regions (Li et al., 2013). Much like ALG-3/4 26G-RNAs, mouse pachytene piRNAs are expressed specifically in developing spermatocytes upon entering the pachytene stage of meiotic prophase I (Girard et al., 2006). Intriguingly, MIWI was shown to associate with the translational machinery as well as with polysomes during early spermiogenesis, leading to speculation that it promotes translation (Lau, 2010). Recent work also suggests that MIWI promotes the stabilization of spermiogenic mRNAs (Nishibu et al., 2012; Vourekas et al., 2012). Interestingly, a protective role for small RNAs and PIWI Argonaute proteins was recently identified in the ciliated protozoan Oxytricha, where piRNAs prevent DNA elimination during genome rearrangement (Fang et al., 2012). These findings raise a thought-provoking possibility that pachytene piRNAs and ALG-3/4/CSR-1 small RNAs provide analogous functions, protecting the genome and buffering gene expression in distant phyla.

Whole-Genome Surveillance by Argonaute/Small RNA Pathways

While ALG-3/4 and CSR-1 function together to promote the expression of many genes required for spermiogenesis, ALG-3/4 also functions independently of CSR-1 to negatively regulate a subset of its targets via the WAGO gene-silencing pathway. Although CSR-1 22G-RNAs target these same mRNAs, CSR-1 is not required for their silencing (Figures S3 and 5). Indeed, perhaps paradoxically, both CSR-1 and ALG-3/4 appear to moderately promote the transcription of these ALG-3/4 negatively regulated targets. These observations suggest that in males ALG-3/4 and CSR-1 promote the transcription of some targets that are silenced posttranscriptionally via the WAGO/22G-RNA pathway. This complexity might reflect distinct positive and negative regulation of the same target genes by CSR-1 and WAGO at different times during spermatogenesis. However, it is also possible that transcriptional upregulation of these targets is required to ensure that sufficient template RNA is produced to reamplify WAGO-22G-RNAs important for posttranscriptional silencing in the next generation. In either case, these findings hint at additional complexity.

Surprisingly, males also contain abundant CSR-1 22G-RNAs targeting female-specific transcripts. We do not know whether these 22G-RNAs are maternal CSR-1/22G-RNA complexes that persist in the male or, alternatively, if they are generated de novo in males, perhaps using transcripts maternally inherited or produced at low levels. Regardless of their origin, this result could indicate that sperm transmit a memory of both paternal and grand-maternal gene expression. CSR-1 is also abundant in oocytes and it seems likely that it could provide similar functions there, delivering epigenetic signals from the mother and possibly the grandfather. Given the relatively much smaller volume of sperm, it is possible that the ALG-3/4 system exists, in part, to amplify the sperm-specific CSR-1 signal, ensuring both the robust expression of sperm genes and the transmission of a memory of sperm-specific gene expression to offspring.

Like CSR-1-dependent small RNA signals, WAGO-dependent signals are also transmitted via both the egg and the sperm (Ashe et al., 2012; Buckley et al., 2012; Gu et al., 2009; Shirayama et al., 2012). Our analysis of CSR-1 and a previous study of HRDE-1/WAGO-9 (Buckley et al., 2012) suggest that both Argonaute pathways promote germline immortality. Interestingly, when either small RNA pathway is lost, fertility begins to decline gradually over a few generations. These findings suggest that Argonautes act to reinforce and maintain parallel transgenerational epigenetic signals that might, for example, be chromatin mediated. In the respective Argonaute mutants, loss of the small RNA signals may cause a gradual loss, over a period of several generations, of chromatin marks associated with active or silent gene-expression states, resulting in the observed gradual onset of germline mortality.

Recent work on transgenes expressed in the *C. elegans* germline (Seth et al., 2013) has identified a CSR-1-dependent transgenerational activating signal (RNAa). This activating signal, which can be transmitted via the sperm, can act within a single generation to reverse a persistent mode of epigenetic silencing referred to as RNA-induced epigenetic gene silencing (RNAe) (Shirayama et al., 2012). Interestingly, while desilencing was observed immediately after exposure to RNAa, continuous exposure, over many generations, was necessary to render a formerly silent gene capable of durable independent expression (Seth et al., 2013). The maintenance of RNAe requires members of the WAGO clade of Argonautes, as well as repressive heterochromatin factors and histone modifications (Ashe et al., 2012; Buckley et al., 2012; Shirayama et al., 2012). Perhaps germline mortality occurs gradually, after loss of CSR-1 and ALG-3/4 activity, as silencing marks spread into and gradually silence genes required for spermatogenesis. The findings reported here support the idea that CSR-1 transmits a protective small RNA-induced *trans*-activating signal and provide physiological evidence linking CSR-1 and RNAa more globally to the transmission and maintenance of paternal, and possibly maternal, epigenetic memory.

EXPERIMENTAL PROCEDURES

Worm Strains and Genetics

C. elegans culture and genetics were performed as described previously (Brenner, 1974). Unless otherwise noted, the wild-type (WT) strain in this study

is the Bristol N2 strain carrying the *fog-2(q71)* allele. Alleles used in this study listed by chromosome. LGI: *fer-1(hc24)*, *fer-1(b232)*, *fer-6(hc23)*, *fer-7(hc34)*; LGII: *neSi1[cb-unc-119(+) 3xflag::csr-1]*, *eri-3(tm1361)*, *fer-3(hc3)*, *rrf-3(pk1426)*, *fer-15(b26)*; LGIII: *alg-4(ok1041)*, *unc-119(ed3)*, *fer-2(hc2)*; LGIV: *alg-3(tm1155)*, *csr-1(tm892)*, *DnT1[unc(n754 dm) let](IV;V)*; LGV: *fog-2(q71)*, *fer-4(hc4)*. The *3xflag::csr-1* transgenic strain was generated by Mos-mediated single-copy insertion (Frøkjaer-Jensen et al., 2008) and details are provided in the Extended Experimental Procedures. Analysis of Eri phenotypes, male fertility and spermatid activation are described in the Extended Experimental Procedures.

Molecular Biology

Males were enriched to >95% homogeneity by filtering through a 35 μm mesh filter (Miller, 2006). Worms were homogenized in a stainless steel Dounce in the presence of TRI Reagent (Molecular Research Center [MRC]) for RNA isolation or IP buffer (Gu et al., 2009) for IP. RNA was extracted in TRI Reagent (MRC) according to the manufacturer's specifications. The FLAG::CSR-1 IP was performed as described previously (Gu et al., 2009; Shirayama et al., 2012) using M2 FLAG antibody (Invitrogen). Details of small RNA cloning and data analyses are provided in the Extended Experimental Procedures. Perl Scripts are available upon request.

Quantitative PCR and Chromatin IP

Reverse transcription followed by qPCR (RT-qPCR) was performed as described (Batista et al., 2008). To measure pre-mRNA, a qPCR primer was placed within intron sequence. A detailed ChIP method, including antibodies used, is provided in the Extended Experimental Procedures. Target enrichment was assayed by qPCR and is relative to a negative control IgG ChIP and a control intergenic region. Primer sequences are available upon request.

Proteomics

Sperm were isolated from *fog-2* males fed with ^{15}N-labeled (or heavy) HB101 bacteria for three generations at 20°C and from *fog-2* or *alg-3/4; fog-2* males fed with unlabeled HB101 bacteria at 20°C or 25°C. Each sperm sample was homogenized and lysates were centrifuged twice at 10,000 × *g* for 20 min. Proteins were precipitated in trichloroacetic acid and washed in acetone. Proteins were denatured, reduced, and alkylated prior to trypsin digestion. The ^{15}N-labeled (or heavy) protein sample served as an internal quantification standard by combining with unlabeled (ie. ^{14}N or light) experimental sperm protein samples. Details of the Multidimensional Protein Identification Technology (MuDPIT) analysis are provided in the Extended Experimental Procedures.

ACCESSION NUMBERS

Data for mRNA and small RNA sequencing are available from the Gene Expression Omnibus under the accession number GSE49672.

SUPPLEMENTAL INFORMATION

Supplemental Information includes Extended Results, Extended Experimental Procedures, five figures, and three tables and can be found with this article online at http://dx.doi.org/10.1016/j.cell.2013.11.032.

ACKNOWLEDGMENTS

We thank the Mello laboratory for helpful discussions, E. Youngman and R. Sharma for experimental support, E. Kittler and the UMass Deep Sequencing Core for Illumina sequencing, P. Furcinitti and the UMass Light Microscopy Core for use of the confocal microscope, and the *Caenorhabditis* Genetics Center for providing strains. J.J.M. and J.R.Y. were supported by the National Center for Research Resources (5P41RR011823-17), National Institute of General Medical Sciences (8 P41 GM103533-17), and National Institute on Aging (R01AG027463-04). C.C.M. is a Howard Hughes Medical Institute Investigator and is supported by NIH grant GM058800.

Received: July 28, 2013
Revised: October 7, 2013
Accepted: November 20, 2013
Published: December 19, 2013

REFERENCES

Ahn, S.H., Kim, M., and Buratowski, S. (2004). Phosphorylation of serine 2 within the RNA polymerase II C-terminal domain couples transcription and 3′ end processing. Mol. Cell *13*, 67–76.

Argon, Y., and Ward, S. (1980). Caenorhabditis elegans fertilization-defective mutants with abnormal sperm. Genetics *96*, 413–433.

Ashe, A., Sapetschnig, A., Weick, E.M., Mitchell, J., Bagijn, M.P., Cording, A.C., Doebley, A.L., Goldstein, L.D., Lehrbach, N.J., Le Pen, J., et al. (2012). piRNAs can trigger a multigenerational epigenetic memory in the germline of C. elegans. Cell *150*, 88–99.

Bagijn, M.P., Goldstein, L.D., Sapetschnig, A., Weick, E.M., Bouasker, S., Lehrbach, N.J., Simard, M.J., and Miska, E.A. (2012). Function, targets, and evolution of Caenorhabditis elegans piRNAs. Science *337*, 574–578.

Batista, P.J., Ruby, J.G., Claycomb, J.M., Chiang, R., Fahlgren, N., Kasschau, K.D., Chaves, D.A., Gu, W., Vasale, J.J., Duan, S., et al. (2008). PRG-1 and 21U-RNAs interact to form the piRNA complex required for fertility in C. elegans. Mol. Cell *31*, 67–78.

Brenner, S. (1974). The genetics of Caenorhabditis elegans. Genetics *77*, 71–94.

Buckley, B.A., Burkhart, K.B., Gu, S.G., Spracklin, G., Kershner, A., Fritz, H., Kimble, J., Fire, A., and Kennedy, S. (2012). A nuclear Argonaute promotes multigenerational epigenetic inheritance and germline immortality. Nature *489*, 447–451.

Burke, D.J., and Ward, S. (1983). Identification of a large multigene family encoding the major sperm protein of Caenorhabditis elegans. J. Mol. Biol. *171*, 1–29.

Buttery, S.M., Ekman, G.C., Seavy, M., Stewart, M., and Roberts, T.M. (2003). Dissection of the Ascaris sperm motility machinery identifies key proteins involved in major sperm protein-based amoeboid locomotion. Mol. Biol. Cell *14*, 5082–5088.

Chu, D.S., Liu, H., Nix, P., Wu, T.F., Ralston, E.J., Yates, J.R., 3rd, and Meyer, B.J. (2006). Sperm chromatin proteomics identifies evolutionarily conserved fertility factors. Nature *443*, 101–105.

Claycomb, J.M., Batista, P.J., Pang, K.M., Gu, W., Vasale, J.J., van Wolfswinkel, J.C., Chaves, D.A., Shirayama, M., Mitani, S., Ketting, R.F., et al. (2009). The Argonaute CSR-1 and its 22G-RNA cofactors are required for holocentric chromosome segregation. Cell *139*, 123–134.

Conine, C.C., Batista, P.J., Gu, W., Claycomb, J.M., Chaves, D.A., Shirayama, M., and Mello, C.C. (2010). Argonautes ALG-3 and ALG-4 are required for spermatogenesis-specific 26G-RNAs and thermotolerant sperm in Caenorhabditis elegans. Proc. Natl. Acad. Sci. USA *107*, 3588–3593.

Deng, W., and Lin, H. (2002). miwi, a murine homolog of piwi, encodes a cytoplasmic protein essential for spermatogenesis. Dev. Cell *2*, 819–830.

Duchaine, T.F., Wohlschlegel, J.A., Kennedy, S., Bei, Y., Conte, D., Jr., Pang, K., Brownell, D.R., Harding, S., Mitani, S., Ruvkun, G., et al. (2006). Functional proteomics reveals the biochemical niche of C. elegans DCR-1 in multiple small-RNA-mediated pathways. Cell *124*, 343–354.

Eddy, E.M. (2002). Male germ cell gene expression. Recent Prog. Horm. Res. *57*, 103–128.

Fang, W., Wang, X., Bracht, J.R., Nowacki, M., and Landweber, L.F. (2012). Piwi-interacting RNAs protect DNA against loss during Oxytricha genome rearrangement. Cell *151*, 1243–1255.

Ghildiyal, M., and Zamore, P.D. (2009). Small silencing RNAs: an expanding universe. Nat. Rev. Genet. *10*, 94–108.

Girard, A., Sachidanandam, R., Hannon, G.J., and Carmell, M.A. (2006). A germline-specific class of small RNAs binds mammalian Piwi proteins. Nature *442*, 199–202.

Gu, W., Shirayama, M., Conte, D., Jr., Vasale, J., Batista, P.J., Claycomb, J.M., Moresco, J.J., Youngman, E.M., Keys, J., Stoltz, M.J., et al. (2009). Distinct argonaute-mediated 22G-RNA pathways direct genome surveillance in the C. elegans germline. Mol. Cell *36*, 231–244.

Gu, W., Lee, H.C., Chaves, D., Youngman, E.M., Pazour, G.J., Conte, D., Jr., and Mello, C.C. (2012). CapSeq and CIP-TAP identify Pol II start sites and reveal capped small RNAs as C. elegans piRNA precursors. Cell *151*, 1488–1500.

Han, T., Manoharan, A.P., Harkins, T.T., Bouffard, P., Fitzpatrick, C., Chu, D.S., Thierry-Mieg, D., Thierry-Mieg, J., and Kim, J.K. (2009). 26G endo-siRNAs regulate spermatogenic and zygotic gene expression in Caenorhabditis elegans. Proc. Natl. Acad. Sci. USA *106*, 18674–18679.

Hirsh, D., and Vanderslice, R. (1976). Temperature-sensitive developmental mutants of Caenorhabditis elegans. Dev. Biol. *49*, 220–235.

Jannes, P., Spiessens, C., Van der Auwera, I., D'Hooghe, T., Verhoeven, G., and Vanderschueren, D. (1998). Male subfertility induced by acute scrotal heating affects embryo quality in normal female mice. Hum. Reprod. *13*, 372–375.

Kelly, W.G., Schaner, C.E., Dernburg, A.F., Lee, M.H., Kim, S.K., Villeneuve, A.M., and Reinke, V. (2002). X-chromosome silencing in the germline of C. elegans. Development *129*, 479–492.

Lau, N.C. (2010). Small RNAs in the animal gonad: guarding genomes and guiding development. Int. J. Biochem. Cell Biol. *42*, 1334–1347.

Lee, H.C., Gu, W., Shirayama, M., Youngman, E., Conte, D., Jr., and Mello, C.C. (2012). C. elegans piRNAs mediate the genome-wide surveillance of germline transcripts. Cell *150*, 78–87.

Li, X.Z., Roy, C.K., Dong, X., Bolcun-Filas, E., Wang, J., Han, B.W., Xu, J., Moore, M.J., Schimenti, J.C., Weng, Z., and Zamore, P.D. (2013). An ancient transcription factor initiates the burst of piRNA production during early meiosis in mouse testes. Mol. Cell *50*, 67–81.

Miller, M.A. (2006). Sperm and oocyte isolation methods for biochemical and proteomic analysis. Methods Mol. Biol. *351*, 193–201.

Nishibu, T., Hayashida, Y., Tani, S., Kurono, S., Kojima-Kita, K., Ukekawa, R., Kurokawa, T., Kuramochi-Miyagawa, S., Nakano, T., Inoue, K., and Honda, S. (2012). Identification of MIWI-associated Poly(A) RNAs by immunoprecipitation with an anti-MIWI monoclonal antibody. Biosci. Trends *6*, 248–261.

Pavelec, D.M., Lachowiec, J., Duchaine, T.F., Smith, H.E., and Kennedy, S. (2009). Requirement for the ERI/DICER complex in endogenous RNA interference and sperm development in Caenorhabditis elegans. Genetics *183*, 1283–1295.

Rando, O.J. (2012). Daddy issues: paternal effects on phenotype. Cell *151*, 702–708.

Reinke, V., Gil, I.S., Ward, S., and Kazmer, K. (2004). Genome-wide germline-enriched and sex-biased expression profiles in Caenorhabditis elegans. Development *131*, 311–323.

Rockett, J.C., Mapp, F.L., Garges, J.B., Luft, J.C., Mori, C., and Dix, D.J. (2001). Effects of hyperthermia on spermatogenesis, apoptosis, gene expression, and fertility in adult male mice. Biol. Reprod. *65*, 229–239.

Ruby, J.G., Jan, C., Player, C., Axtell, M.J., Lee, W., Nusbaum, C., Ge, H., and Bartel, D.P. (2006). Large-scale sequencing reveals 21U-RNAs and additional microRNAs and endogenous siRNAs in C. elegans. Cell *127*, 1193–1207.

Sassone-Corsi, P. (2002). Unique chromatin remodeling and transcriptional regulation in spermatogenesis. Science *296*, 2176–2178.

Setchell, B.P., D'Occhio, M.J., Hall, M.J., Laurie, M.S., Tucker, M.J., and Zupp, J.L. (1988). Is embryonic mortality increased in normal female rats mated to subfertile males? J. Reprod. Fertil. *82*, 567–574.

Seth, M., Shirayama, M., Gu, W., Ishidate, T., Conte, D., Jr., and Mello, C.C. (2013). The *C. elegans* CSR-1 Argonaute pathway counteracts epigenetic silencing to promote germline gene expression. Dev. Cell. Published online December 19, 2013. http://dx.doi.org/10.1016/j.devcel.2013.11.014.

Shakes, D.C., Wu, J.C., Sadler, P.L., Laprade, K., Moore, L.L., Noritake, A., and Chu, D.S. (2009). Spermatogenesis-specific features of the meiotic program in Caenorhabditis elegans. PLoS Genet. *5*, e1000611.

Shirayama, M., Seth, M., Lee, H.C., Gu, W., Ishidate, T., Conte, D., Jr., and Mello, C.C. (2012). piRNAs initiate an epigenetic memory of nonself RNA in the C. elegans germline. Cell *150*, 65–77.

Vasale, J.J., Gu, W., Thivierge, C., Batista, P.J., Claycomb, J.M., Youngman, E.M., Duchaine, T.F., Mello, C.C., and Conte, D., Jr. (2010). Sequential rounds of RNA-dependent RNA transcription drive endogenous small-RNA biogenesis in the ERGO-1/Argonaute pathway. Proc. Natl. Acad. Sci. USA *107*, 3582–3587.

Vourekas, A., Zheng, Q., Alexiou, P., Maragkakis, M., Kirino, Y., Gregory, B.D., and Mourelatos, Z. (2012). Mili and Miwi target RNA repertoire reveals piRNA biogenesis and function of Miwi in spermiogenesis. Nat. Struct. Mol. Biol. *19*, 773–781.

Ward, S., Argon, Y., and Nelson, G.A. (1981). Sperm morphogenesis in wild-type and fertilization-defective mutants of Caenorhabditis elegans. J. Cell Biol. *91*, 26–44.

Washington, N.L., and Ward, S. (2006). FER-1 regulates Ca2+ -mediated membrane fusion during C. elegans spermatogenesis. J. Cell Sci. *119*, 2552–2562.

Wu, J.C., Go, A.C., Samson, M., Cintra, T., Mirsoian, S., Wu, T.F., Jow, M.M., Routman, E.J., and Chu, D.S. (2012). Sperm development and motility are regulated by PP1 phosphatases in Caenorhabditis elegans. Genetics *190*, 143–157.

Wykes, S.M., and Krawetz, S.A. (2003). The structural organization of sperm chromatin. J. Biol. Chem. *278*, 29471–29477.

Yigit, E., Batista, P.J., Bei, Y., Pang, K.M., Chen, C.C., Tolia, N.H., Joshua-Tor, L., Mitani, S., Simard, M.J., and Mello, C.C. (2006). Analysis of the C. elegans Argonaute family reveals that distinct Argonautes act sequentially during RNAi. Cell *127*, 747–757.

Cell

EXTENDED RESULTS

The fer Genes Are Required for ALG-3/4 26G-RNAs

Mutations in the Argonautes ALG-3/4 and in other enhanced RNAi (ERI) pathway components exhibit a temperature-sensitive sperm-defective phenotype (Conine et al., 2010; Han et al., 2009; Pavelec et al., 2009). At 20°C, *alg-3/4* mutant males produce many functional spermatozoa and are able to produce a brood size equal to approximately 50% (~150) of WT levels. However, at 25°C they produce haploid spermatids that fail to undergo spermiogenesis, the postmeiotic differentiation process where a pseudopod is formed thus creating spermatozoa competent for fertilization. At 25°C, *alg-3/4* spermatids occasionally make aberrant, multi-branched "spiked" pseudopods, but normally no activation is seen (Conine et al., 2010) which results in arrest as round-spermatids and complete male-specific sterility at 25°C.

To better characterize the spermiogenesis defect of *alg-3/4* mutants, we used transmission electron microscopy (TEM) to examine *alg-3/4* spermatozoa at an ultrastructural level (Figure 1A). WT *C. elegans* spermatids and spermatozoa exhibit several striking features that are visible using TEM. These include an electron-dense perinuclear halo containing RNA that encases the nucleus and centrosome of the spermatids and persists through spermiogenesis in spermatozoa (Ward et al., 1981), as well as the Fibrous Body (FB)-Membraneous Organelle (MO) complex (FB-MO) (Roberts et al., 1986) (Figure 1). The morphogenesis of FB-MOs begins in 1° spermatocytes, where large organelles derived from the Golgi become associated with fibrous bodies comprised of polymerized Major Sperm Protein (MSP), the major structural component of the pseudopod (Roberts et al., 1986; Ward and Klass, 1982). In haploid spermatids, MOs localize to the plasma membrane while FBs dissolve, releasing depolymerized MSP into the cytoplasm. During spermiogenesis or activation of the spermatid the MOs fuse with the plasma membrane on one side of the spermatid, releasing their contents from the cell for oocyte signaling, while MSP protein polymerizes to form the pseudopod on the opposite pole.

At 20°C many *alg-3/4* spermatozoa form WT-looking pseudopods. However, MOs fail to become polarized and often fuse with the plasma membrane adjacent to the pseudopod rather than with the outer membrane on the opposite side of the spermatid (Figure 1). At 25°C *alg-3/4* spermatids never form a WT pseudopod and the RNA halo is frequently absent or appears abnormal. In addition, large tubule-like structures are present in the cytoplasm (Figure 1). These tubules are too large in diameter to be comprised of known cytoskeletal components, but instead are thought to be made up of polymerized perinuclear halo components (Ward et al., 1981). We also found that FBs fail to disassemble in *alg-3/4* mutants at 25°C (Figure 1), a phenotype characteristic of *fer-6* spermatozoa, which also fail to make pseudopods (Ward et al., 1981).

The fertility and ultrastructural phenotypes of *alg-3/4* mutant sperm are identical to those of temperature-sensitive fertilization-defective (*fer*) mutants isolated in genetic screens more than 30 years ago (Argon and Ward, 1980; Hirsh and Vanderslice, 1976; Ward et al., 1981). To date, most of the *fer* genes remain molecularly uncharacterized except for *fer-1*, which encodes a member of the Ferlin family of membrane proteins required for the fusion of MOs during spermiogenesis (Washington and Ward, 2006).

Considering the similarity of *alg-3/4* and *fer* mutant phenotypes, we asked whether the WT activities of the *fer* genes are required for the production of ALG-3/4 pathway 26G-RNAs. Northern blot analysis of small RNAs isolated from L4/Young adult staged hermaphrodites revealed that *fer-2*, *−4*, *−6*, and *-15* are required for the production of two abundant ALG-3/4 pathway 26G-RNAs targeting the mRNA products of *f36h12.4* and *ssp-16* (Figure S1A). In the *fer-3* mutant, 26G-RNAs targeting *f36h12.4* and *ssp-6* were significantly reduced or absent, suggesting that *fer-3(hc3)* may be a hypomorphic allele of a gene required for 26G-RNA biogenesis. Neither *fer-1* nor *fer-7* were required for the expression of either *f36h12.4* or *ssp-6* 26G-RNAs (Figure S1A). Consistent with this finding, *fer-1* and *fer-7* appear to act later in sperm development than *alg-3/4* and the remaining *fer* mutants tested here (Argon and Ward, 1980; Conine et al., 2010). Furthermore, *fer-1* mutant spermatozoa form short-stubby pseudopods with normal looking projections at 25°C, whereas *alg-3/4* and *fer-2*, *−4*, *−6*, and *-15* mutant spermatozoa do not develop pseudopods at 25°C (Ward et al., 1981).

We found that *fer-3(hc3)* and *fer-15(b26)* exhibit an Eri phenotype (Figure S1B) and, like other Eri mutants, are required for ERGO-1 pathway 26G-RNAs targeting the gene *c44b11.6* (Figure S1A). Indeed, *fer-3* and *fer-15* mutations map nearby the ERI-pathway genes *eri-3* and *rrf-3*, respectively (Roberts and Ward, 1982; Ward et al., 1981). *fer-3(hc3)* failed to complement the Fer and Eri phenotypes of *eri-3(tm1361)* (Figure S1B). Consistent with this finding, and the partial loss of male-specific 26G-RNAs, we identified a nucleotide substitution in exon 3 of *eri-3* that is predicted to result in a serine-to-proline missense mutation at amino acid 69 (Figure S1C). *fer-15(b26)* failed to complement the Fer and Eri phenotypes of *rrf-3(pk1426)*, and we identified a 223 bp deletion that removes exon 6 of *rrf-3* and is predicted to shift the reading frame and introduce a premature termination codon (Figure S1C). *fer-2*, *fer-4* and *fer-6* mutants were not Eri, and their molecular identities remain to be determined. Taken together, our findings indicate that several previously isolated Fer mutants define genes that function in the ALG-3/4-26G-RNA pathway.

Target Regulation by ALG-3/4: mRNA-Seq and Proteomic Analyses

To determine how ALG-3/4 and 26G-RNAs regulate target mRNAs, we performed mRNA deep sequencing (mRNA-seq) of poly-A purified mRNA isolated from WT and *alg-3/4* mutant males grown at 20° and 25°C. Comparing the relative levels of ALG-3/4 targeted mRNAs between *alg-3/4* mutant males and WT males cultured at 25°C, we found that 204 target mRNAs increased ≥ 2-fold in the *alg-3/4* mutant, suggesting that these target mRNAs are negatively regulated by ALG-3/4 (Figure 2A and Table S1). Strikingly, 214 target genes decreased by ≥ 2-fold (Figure 2A and Table S1), suggesting that they are positively regulated by ALG-3/4.

To determine whether the changes in male mRNA expression correlate with changes in the sperm proteome, we compared the proteomes of *alg-3/4* mutant spermatids and WT spermatids purified from males grown at 20°C or 25°C. To do this, we used stable isotope labeling by amino acids (Ong et al., 2002) to label WT proteins with the heavy isotope of nitrogen, ^{15}N. Unlabeled protein extracted from *alg-3/4* or WT sperm was combined with a known quantity of labeled WT sperm protein, and the mixture was analyzed by mass spectrometry (Moresco et al., 2010). For each mixture, we obtained a ratio of unlabeled peptides (from *alg-3/4* or WT at 20°C or 25°C) to labeled peptides (from WT sperm at 20°C) for each protein, which allowed us to measure relative protein levels between *alg-3/4* mutant and WT sperm, or between temperatures. Focusing on the ALG-3/4 26G-RNA targets, we found that 43 target proteins increased by $\geq$ 1.5-fold in *alg-3/4* mutant sperm at 25°C relative to WT sperm, suggesting that these targets are negatively regulated by ALG-3/4. However, 122 target proteins decreased by $\geq$ 1.5-fold in *alg-3/4* mutant sperm, suggesting that they are positively regulated by ALG-3/4 (Figure S2A and Table S2). These findings were consistent with our mRNA-seq analysis: 35% (14/43) of negatively regulated proteins were also negatively regulated by $\geq$ 1.5-fold at the mRNA level, while 66% (81/122) of positively regulated proteins were also positively regulated by $\geq$ 1.5-fold at the mRNA level. These data indicate that ALG-3/4 promotes expression of positively regulated targets at the mRNA level.

CSR-1 Associates with Small RNAs Targeting Female-Specific mRNAs in the Male Germline

Surprisingly, while analyzing our CSR-1 IP data, we found that the FLAG::CSR-1 IP from males enriched small RNAs that target female-specific genes (Reinke et al., 2004). Remarkably, these oogenesis-specific small RNAs were present at levels similar to those of small RNAs targeting male-specific genes (Figure 5D). This finding is striking given that the corresponding female-specific mRNAs were at least 13-fold less abundant than male-specific mRNAs in our mRNA-seq data (Figure 5D). These results suggest that males might inherit maternally derived small RNAs that target female-specific genes and actively transmit them to their offspring (see Discussion).

EXTENDED EXPERIMENTAL PROCEDURES

Eri, Fertility, and Spermatid Activation Assays

Eri phenotypes were assayed by feeding worms with bacteria expressing *unc-73* dsRNA and scoring the F1 progeny for the Unc-73 phenotype (Duchaine et al., 2006; Kennedy et al., 2004). Male fertility was assayed by mating males to virgin *fog-2* females and determining the number of viable cross progeny as described (Batista et al., 2008). Spermatid activation was performed by isolated spermatids from males and incubating with 200 μg/ml pronase as described (Shakes and Ward, 1989).

Molecular Biology

The *flag::csr-1* transgene was generated by Mos-mediated single copy insertion (Frøkjaer-Jensen et al., 2008). A 7.0 kb SpeI – BstZ171 fragment from cosmid F20D12 containing the entire *csr-1* gene was inserted into a modified version of pCFJ151 (B1496) for insertion into LGII (Frøkjaer-Jensen et al., 2008). The *3xflag* sequence was inserted into a SmaI site created by site-direct mutagenesis immediately after the initiation codon in the second exon of the *csr-1* gene. The *3xflag::csr-1* vector was present at 10 ng/ml in the MosSCI injection mixture. Expression of FLAG::CSR-1 was confirmed by western blot. The single copy *3xflag::csr-1* transgene inserted in LGII fully rescued the *csr-1(tm892)* null mutant.

Males were enriched to > 95% homogeneity by filtering through a 35 micron mesh filter (Miller, 2006). Worms were homogenized in a stainless steel dounce homogenizer in the presence of TRI Reagent (MRC Inc) for RNA isolation or IP buffer (Gu et al., 2009) for IP analyses. RNA was extracted in TRI Reagent (MRC Inc) according to the manufacturer's specifications. The FLAG::CSR-1 IP for small RNA cloning was performed essentially as described (Gu et al., 2009; Shirayama et al., 2012) using M2 FLAG antibody (Invitrogen).

Small RNA enrichment and Northern blots were performed as described (Conine et al., 2010). For cloning and deep sequencing, small RNAs were pretreated with Tobacco Acid Pyrophosphatase (Epicenter Biotechnologies) and ligated to an adenylated 3′ linker and then to a 5′ linker containing a 4 nt barcode as described (Gu et al., 2009). Illumina adapters were added by PCR. For mRNA sequencing, polyA RNA was purified from total RNA using the PolyATtract mRNA Isolation System (Promega); each sample was purified twice. The mRNA was fragmented by base hydrolysis at 65°C for 9.5 min in Sodium carbonate buffer, and 2′,3′-cyclic phosphates were resolved with T4 Polynucleotide Kinase (NEB). mRNA fragments with an average length of ~200 nt were purified from an 8% polyacrylamide/8 M urea gel, ligated to a 3′ linker, and reverse transcribed (Superscript III, Invitrogen) using a primer targeting the 3′ linker and containing reverse complement 5′ linker sequence with barcodes for multiplex sequencing. The cDNA was circularized using Circligase (epicenter).

Illumina adapters were added by PCR and cDNA libraries were sequenced by the UMass Deep Sequencing Core using an Illumina GAII or HiSeq. Deep-sequencing data analyses were performed as described (Gu et al., 2012). RPMK analysis was performed on the mRNA-seq libraries using a custom Perl script. Perl Scripts are available upon request.

Quantitative PCR and Chromatin IP

Reverse transcription followed by qPCR (RT-qPCR) was performed as described (Batista et al., 2008). To measure pre-mRNA, one of the RT-qPCR primers was placed within intron sequence. Primer sequences are available upon request.

For ChIP, male worms were enriched to >95%, crosslinked in 2% paraformaldehyde for 30 min at 20°C, washed and worm pellets were flash frozen. Worm pellets were resuspended in 4 volumes of FA buffer (Cold Spring Harbor Protocols) containing protease inhibitors (Roche) and sonicated at medium intensity in a Bioruptor (Diogenode) for 50 min (30 s on, 30 s off). Insoluble debris was pelleted by centrifugation at 13,000 x g for 15 min. For Pol II ChIP, 6μg of mouse monoclonal anti-Pol II RNA pol II (8WG16 from Covance) was added to 5 mg of protein lysate and incubated for 2 hr at 4°C. For CSR-1 ChIP, 10 μg of anti-CSR-1 antibody (Claycomb et al., 2009) was added to 10-15 mg of protein lysate and incubated for 2 hr at 4°C. Immune complexes were captured with protein A/G agarose beads (Santa Cruz) at 4°C for 2 hr and washed, and proteins were eluted in TE containing 1% SDS and 250 mM NaCl at 65°C for 15 min in a thermomixer (800-1000 rpm). As an IgG negative control, 6 μg of normal mouse IgG (Santa Cruz) was also added to 5 mg of protein lysate, and processed the same as the experimental samples. Crosslinks were reversed by incubating overnight in TE/1% SDS at 65°C, and proteins were digested with proteinase K. DNA was extracted with phenol-chloroform and precipitated with ethanol. Enrichment of target loci was assayed by qPCR relative to the negative control IgG ChIP and a control intergenic region.

Fluorescence Microscopy

Male germlines were dissected on poly-lysine slides in PBS, fixed in methanol and formaldehyde and washed with PBT (PBS, 0.1% BSA, and 0.1% Triton X-100). For immunofluorescence, slides were incubated with primary antibodies in PBT overnight at 4°C, washed with PBT, and incubated with secondary antibody in PBT for 1-2 hr at room temperature. Slides were washed and mounted with Vectashield (Vector) containing 1 μg/ml DAPI. The following primary antibodies were used in this study: anti-MSP (4A5 from DSHB), anti-GSP-3 (kind gift from Dr. Diana Chu; Wu et al., 2012), anti-elongating RNA pol II (H5 from Covance), anti-CSR-1(Claycomb et al., 2009), anti-nuclear pore (MAB414 from Covance), and anti-H3K4me2 (07-030 Millipore). Secondary antibodies were obtained from Jackson Immunoresearch or Molecular Probes. For mRNA FISH, slides were hybridized with Stellaris RNA FISH probes (Biosearch Technologies) and processed for imaging according to the manufacturer's recommendations for *C. elegans* samples.

The number of condensing nuclei in *alg-3/4* and *csr-1* male germlines was determined using DAPI images from immunofluorescence and RNA FISH experiments by counting all of the nuclei from pachytene to metaphase of the first meiotic division in which chromosomes could not be individually resolved.

Images were acquired with a Solamere Technology Group CSU10B Spinning Disk Confocal System scan head mounted on a Nikon TE-200E2 inverted microscope with a 60X or 100X Plan/APO Oil lens and a Roper Coolsnap HQ2 camera. Images were processed using Metamorph (7.7.4), ImageJ (1.47n5), and Adobe Photoshop (CS4) software. Z sections with slices ranging from 0.2 to 0.4 μm were collected.

Proteomics

Sperm were isolated from *fog-2* males fed with ^{15}N-labeled (or heavy) HB101 bacteria for three generations at 20°C and from *fog-2* or *alg-3/4; fog-2* males fed with unlabeled HB101 bacteria at 20°C or 25°C. Each sperm sample was homogenized and lysates were centrifuged twice at 10,000 x *g* for 20 min. Proteins were precipitated in trichloroacetic acid and washed in acetone. Proteins were denatured, reduced and alkylated prior to trypsin digestion. The ^{15}N-labeled (or heavy) protein sample served as an internal quantification standard by combining with unlabeled (ie. ^{14}N or light) experimental sperm protein samples. MuDPIT (Washburn et al., 2001) analyses were performed using an Eksigent nano-LC pump and a Thermo LTQ-Orbitrap connected to a homemade electrospray stage. Protein identification and quantification were performed with Integrated Proteomics Pipeline - IP2 (Integrated Proteomics Applications, Inc., San Diego, CA. http://www.integratedproteomics.com/). Tandem mass spectra were extracted from raw files using RawExtract 1.9.9 (McDonald et al., 2004), searched against the Wormbase protein database (release WP180) and reversed sequences using ProLuCID (Peng et al., 2003; Xu et al., 2006), and peptide candidates were filtered using DTASelect with the parameters –p 1 –y 1 –trypstat –DM 10 –in (McDonald et al., 2004; Tabb et al., 2002). Quantification was performed using Census (Park et al., 2008).

Reagents and Chemicals

Deionized water (18.2 MΩ, Barnstead, Dubuque, IA) was used for all preparations. Buffer A consists of 5% acetonitrile 0.1% formic acid, buffer B consists of 80% acetonitrile 0.1% formic acid, and buffer C consists of 500 mM ammonium acetate and 5% acetonitrile.

Sample Preparation

Fifty μg each of light and heavy proteins were mixed and brought to 200 μl with water. Proteins were precipitated with 60 μl TCA (Sigma-Aldrich, St. Louis, MO, Product number T-0699) at 4°C O/N. After 30 min centrifugation at 18,000 x g, protein pellets were washed 2 times with 500 μl ice-cold acetone. Air-dried pellets were dissolved in 8 M urea/ 100 mM Tris pH 8.5. Proteins were reduced with 5 mM Tris(2-carboxyethyl)phosphine hydrochloride (Sigma-Aldrich, St. Louis, MO, product C4706) and alkylated with 10 mM iodoacetamide (Sigma-Aldrich, St. Louis, MO, product I11490). Proteins were digested for 18 hr at 37°C in 2 M urea 100 mM Tris pH 8.5, 1 mM $CaCl_2$ with 2 μg trypsin (Promega, Madison, WI, product V5111). Digest was stopped with formic acid, 5% final concentration. Debris was removed by centrifugation, 30 min 18,000 x g.

MudPIT Microcolumn

A MudPIT microcolumn (Wolters et al., 2001) was prepared by first creating a Kasil frit at one end of an undeactivated 250 μm ID/360 μm OD capillary (Agilent Technologies, Inc., Santa Clara, CA). The Kasil frit was prepared by briefly dipping a 20-30 cm

capillary in well-mixed 300 μL Kasil 1624 (PQ Corporation, Malvern, PA) and 100 μL formamide, curing at 100°C for 4 hr, and cutting the frit to ~2 mm in length. Strong cation exchange particles (SCX Luna, 5 μm dia., 125 Å pores, Phenomenex, Torrance, CA) were packed in-house from particle slurries in methanol 2.5 cm. An additional 2.5 cm reversed phase particles (C18 Aqua, 3 μm dia., 125 Å pores, Phenomenex) were then similarly packed into the capillary using the same method as SCX loading, to create a biphasic column. An analytical RPLC column was generated by pulling a 100 μm ID/360 μm OD capillary (Polymicro Technologies, Inc, Phoenix, AZ) to 5 μm ID tip. Reversed phase particles (Aqua C18, 3 μm dia., 125 Å pores, Phenomenex, Torrance, CA) were packed directly into the pulled column at 800 psi until 12 cm long. The MudPIT microcolumn was connected to an analytical column using a zero-dead volume union (Upchurch Scientific (IDEX Health & Science), P-720-01, Oak Harbor, WA).

LC-MS/MS analysis was performed using an Eksigent nano-LC pump and a Thermo LTQ-Orbitrap using an in-house built electrospray stage. MudPIT experiments were performed where each step corresponds to 0, 10, 20, 30, 40, 50, 60, 70, and 100% buffer C being run for 4 min at the beginning of each gradient of buffer B. The 100% buffer C step was repeated. Electrospray was performed directly from the analytical column by applying the ESI voltage at a tee (150 μm ID, Upchurch Scientific). Electrospray directly from the LC column was done at 2.5 kV with an inlet capillary temperature of 250°C. Data-dependent acquisition of MS/MS spectra with the LTQ -Orbitrap were performed with the following settings: MS/MS on the 6 most intense ions per precursor scan, 1 microscan, charge state 1 reject; dynamic exclusion repeat count, 1, repeat duration, 30 s; exclusion list size 500; and exclusion duration, 180 s.

Data Analysis

Protein and peptide identification and protein quantitation were done with Integrated Proteomics Pipeline - IP2 (Integrated Proteomics Applications, Inc., San Diego, CA.) Tandem mass spectra were extracted from raw files using RawExtract 1.9.9 (McDonald et al., 2004) and were searched against Wormbase database (WP180) with reversed sequences using ProLuCID (Peng et al., 2003; Xu et al., 2006). The search space included all fully tryptic peptide candidates. Carbamidomethylation (+57.02146) of cysteine was considered as a static modification. Peptide candidates were filtered using DTASelect, with these parameters –p 1 –y 1 –trypstat –DM 10 –in (McDonald et al., 2004; Tabb et al., 2002). Quantitation was performed using Census (Park et al., 2008).

SUPPLEMENTAL REFERENCES

Frøkjaer-Jensen, C., Davis, M.W., Hopkins, C.E., Newman, B.J., Thummel, J.M., Olesen, S.P., Grunnet, M., and Jorgensen, E.M. (2008). Single-copy insertion of transgenes in Caenorhabditis elegans. Nat. Genet. *40*, 1375–1383.

Kennedy, S., Wang, D., and Ruvkun, G. (2004). A conserved siRNA-degrading RNase negatively regulates RNA interference in C. elegans. Nature *427*, 645–649.

McDonald, W.H., Tabb, D.L., Sadygov, R.G., MacCoss, M.J., Venable, J., Graumann, J., Johnson, J.R., Cociorva, D., and Yates, J.R., 3rd. (2004). MS1, MS2, and SQT-three unified, compact, and easily parsed file formats for the storage of shotgun proteomic spectra and identifications. Rapid Commun. Mass Spectrom. *18*, 2162–2168.

Moresco, J.J., Carvalho, P.C., and Yates, J.R., 3rd. (2010). Identifying components of protein complexes in C. elegans using co-immunoprecipitation and mass spectrometry. J. Proteomics *73*, 2198–2204.

Ong, S.E., Blagoev, B., Kratchmarova, I., Kristensen, D.B., Steen, H., Pandey, A., and Mann, M. (2002). Stable isotope labeling by amino acids in cell culture, SILAC, as a simple and accurate approach to expression proteomics. Mol. Cell. Proteomics *1*, 376–386.

Park, S.K., Venable, J.D., Xu, T., and Yates, J.R., 3rd. (2008). A quantitative analysis software tool for mass spectrometry-based proteomics. Nat. Methods *5*, 319–322.

Peng, J., Elias, J.E., Thoreen, C.C., Licklider, L.J., and Gygi, S.P. (2003). Evaluation of multidimensional chromatography coupled with tandem mass spectrometry (LC/LC-MS/MS) for large-scale protein analysis: the yeast proteome. J. Proteome Res. *2*, 43–50.

Roberts, T.M., and Ward, S. (1982). Membrane flow during nematode spermiogenesis. J. Cell Biol. *92*, 113–120.

Roberts, T.M., Pavalko, F.M., and Ward, S. (1986). Membrane and cytoplasmic proteins are transported in the same organelle complex during nematode spermatogenesis. J. Cell Biol. *102*, 1787–1796.

Shakes, D.C., and Ward, S. (1989). Initiation of spermiogenesis in C. elegans: a pharmacological and genetic analysis. Dev. Biol. *134*, 189–200.

Tabb, D.L., McDonald, W.H., and Yates, J.R., 3rd. (2002). DTASelect and Contrast: tools for assembling and comparing protein identifications from shotgun proteomics. J. Proteome Res. *1*, 21–26.

Xu, T., Venable, J.D., Park, S.K., Cociorva, D., Lu, B., Liao, L., Wohlschlegel, J., Hewel, J., and Yates, J.R., I. (2006). ProLuCID, a fast and sensitive tandem mass spectra-based protein identification program. Mol. Cell. Proteomics *5*, S174.

Ward, S., and Klass, M. (1982). The location of the major protein in Caenorhabditis elegans sperm and spermatocytes. Dev. Biol. *92*, 203–208.

Washburn, M.P., Wolters, D., and Yates, J.R., 3rd. (2001). Large-scale analysis of the yeast proteome by multidimensional protein identification technology. Nat. Biotechnol. *19*, 242–247.

Wolters, D.A., Washburn, M.P., and Yates, J.R., 3rd. (2001). An automated multidimensional protein identification technology for shotgun proteomics. Anal. Chem. *73*, 5683–5690.

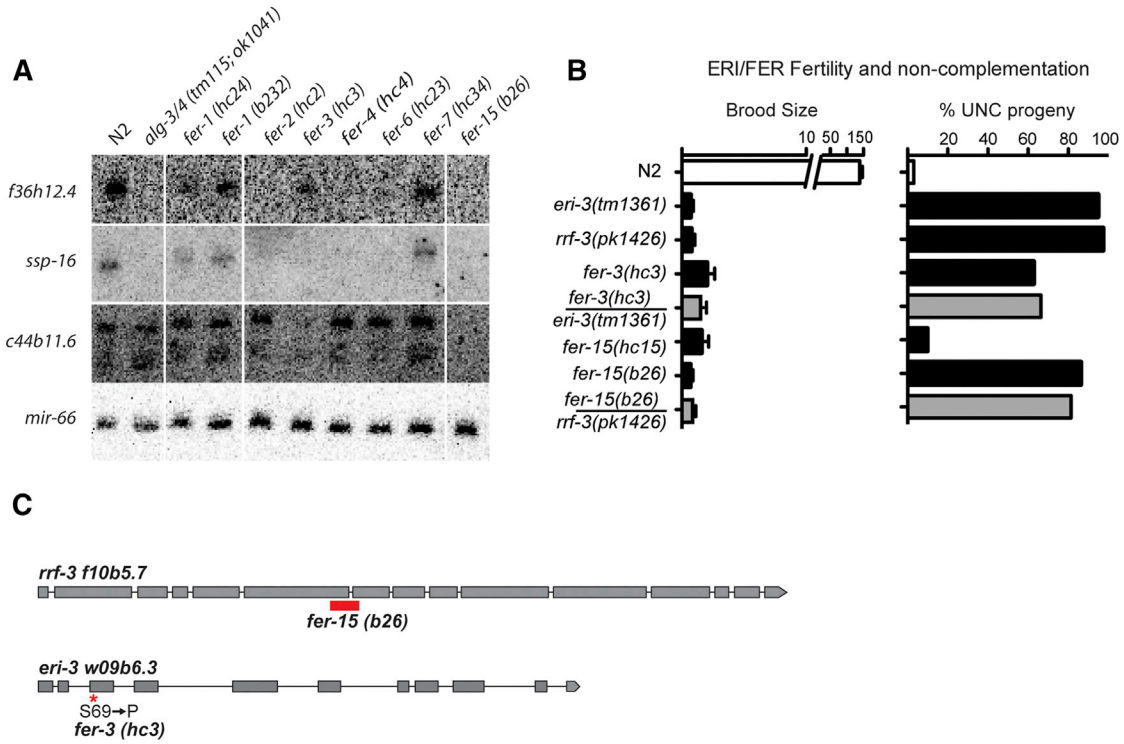

Figure S1. Identification of *fer* Genes as ALG-3/4 Pathway Components, Related to Figure 1

(A) Northern blot analysis of small RNAs from whole L4/Young Adult RNA extracts. Radiolabeled probes were used for two ALG-3/4 targets, *f36h12.4* and *ssp-16*, and for the ERGO-1–dependent 26G-RNA target *c44b11.6*. 22G-RNAs are also visible targeting *c44b11.6*. *mir-66* was probed as a loading control.

(B) Genetic complementation tests for the fertility (Fer) (left panel) and Enhanced RNAi, (Eri) phenotypes (right panel) between *fer-3* and *eri-3* and *fer-15* and *rrf-3*. Fertility was assayed at 25°C. Enhanced RNAi was assayed by *unc-73(RNAi)* feeding.

(C) The exon-intron structures of *rrf-3* and *eri-3* are indicated by the boxes and lines, respectively. The *fer-15(b26)* allele corresponds to a 223 nt deletion (red box) that spans intron 6, results in a frame shift and introduces a premature termination codon in the *rrf-3* coding region The *fer-3(hc3)* corresponds to a missense mutation in *eri-3* that changes Serine 69 to Proline.

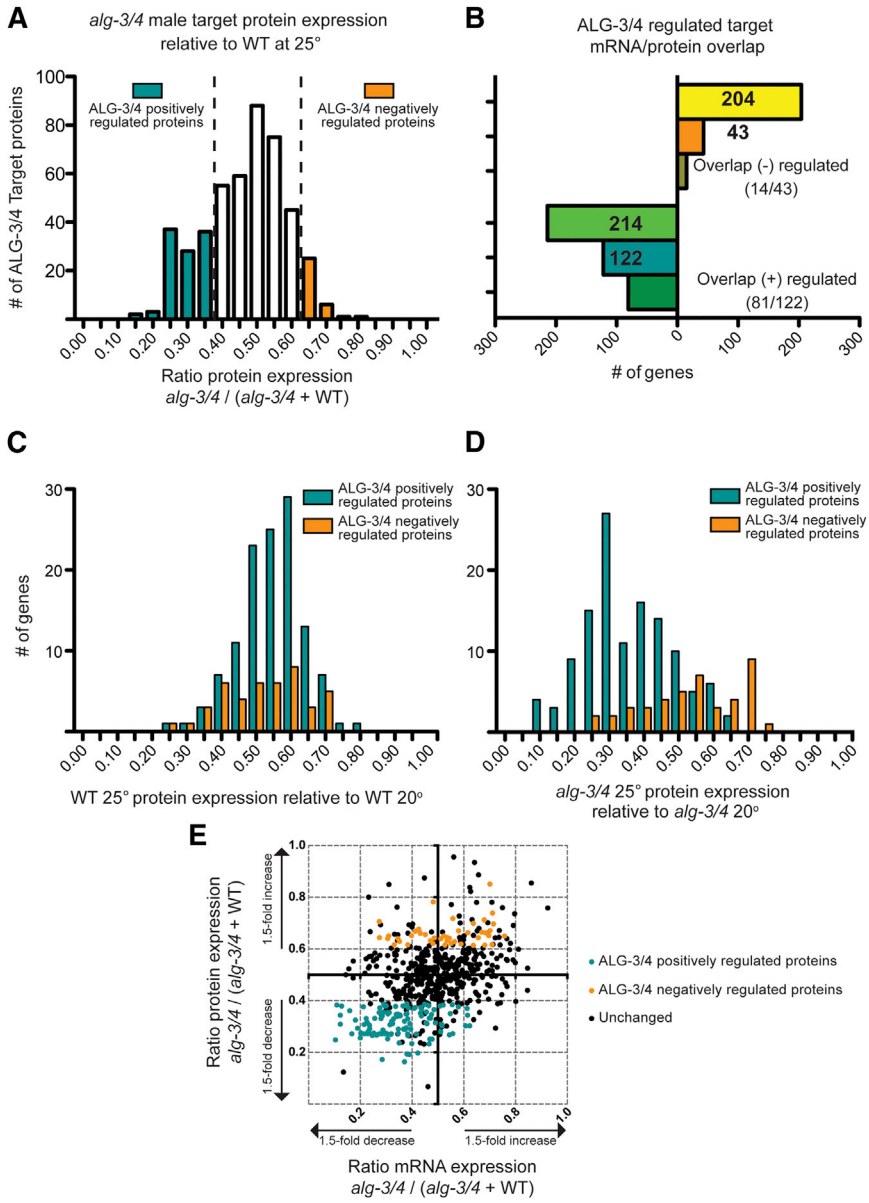

Figure S2. Quantitative Proteomic Analysis of ALG-3/4 Targets in Isolated Sperm, Related to Figure 2

(A) Histogram illustrating the distribution of ALG-3/4 target protein expression in *alg-3/4* mutant sperm relative to WT sperm at 25°C, calculated by peptide ratio in *alg-3/4* divided by the peptide ratio in *alg-3/4* plus the peptide ratio in WT. Dotted lines represent either 2-fold enrichment (right, orange) or depletion (left, turquois) in *alg-3/4*.

(B) Overlap between the ALG-3/4 positively regulated proteins with the positively regulated mRNAs. As well as the ALG-3/4 negatively regulated proteins with the negatively regulated mRNAs.

(C) Histogram illustrating the distribution of ALG-3/4 target protein expression from WT sperm grown at 25°C relative to WT sperm at 20°C, calculated as the peptide ratio in WT 25°C divided by peptide ratio in WT 25°C plus the peptide ratio in WT 20°C.

(D) Histogram illustrating the distribution of ALG-3/4 target protein expression in *alg-3/4* sperm grown at 25°C relative to *alg-3/4* sperm at 20°C.

(E) Scatter plot comparing the expression of proteins (proteomic analysis) in *alg-3/4* sperm relative to WT at 25°C (y axis) to the expression of mRNAs (mRNA-seq) in *alg-3/4* males relative to WT at 25°C (x axis). Turquois dots represent ALG-3/4 positively regulated proteins and orange dots represent ALG-3/4 negatively regulated proteins.

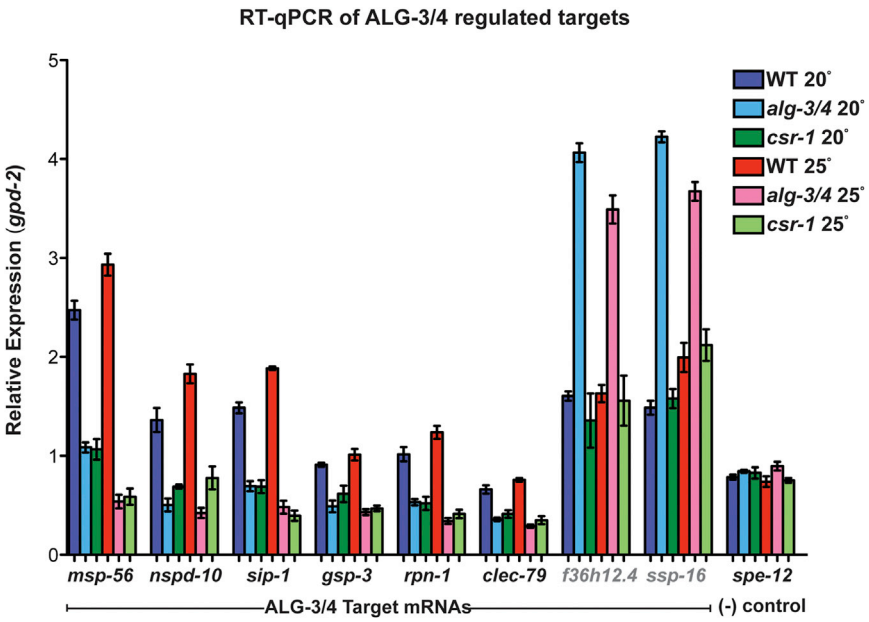

Figure S3. Target mRNA Regulation by ALG-3/4 and CSR-1, Related to Figures 2 and 5

RT-qPCR analysis of ALG-3/4 targets normalized to *gpd-2*. Data are represented as mean ± SEM.

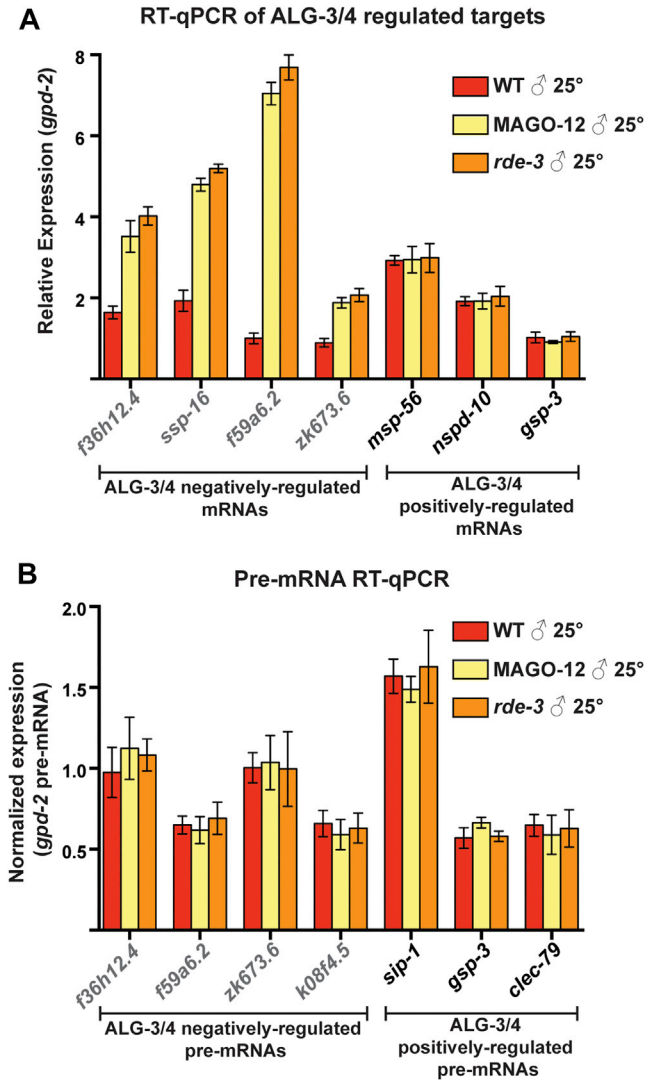

Figure S4. ALG-3/4 Negatively Regulated Targets Are Silenced by the WAGO Small RNA Pathway, Related to Figure 4

(A) RT-qPCR analysis of ALG-3/4 targets normalized to *gpd-2* in WAGO- pathway mutants.

(B) RT-qPCR analysis of ALG-3/4 target pre-mRNAs in WAGO pathway mutants. Values are normalized to the non-target *gpd-2* pre-mRNA. Data are represented as mean ± SEM.

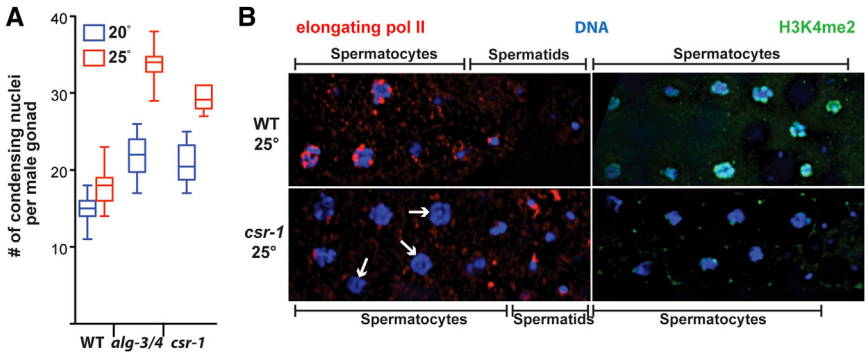

Figure S5. ALG-3/4/CSR-1 Pathway Mutants Exhibit Defects in Spermatogenic Chromatin Condensation and Transcription, Related to Figure 5

(A) *alg-3/4* and *csr*-1 mutants exhibit similar defects in spermatogenic nuclear condensation. Comparison of the number of condensing nuclei present in the meiotic germline of WT, *alg-3/4* and *csr-1* males at 20°C or 25°C. Box and whisker plots indicate the range of data from at least twelve DAPI-stained confocal image stacks per strain and condition.

(B) Confocal IF images of dissected WT (top) or *csr-1* (bottom) spermatogenic germlines at 25°C stained with antibodies against (left) elongating RNA pol II (red), spermatocyte nuclei completely missing pol II staining are denoted with a white arrow, or (right) antibodies against H3K4me2 (green). DNA was stained with DAPI (blue).

See also Figure S3 and Table S3.